lajss.org
Latin American Journal of Solids and Structures
www.lajss.org

The uncertain free vibration analysis of functionally graded sandwich plates placed on a variable elastic foundation

Ngoc-Tu Do[a], Nhan Thinh Hoang[b*]

[a]Faculty of Industrial Systems, School of Mechanical and Automotive Engineering, Hanoi University of Industry, Hanoi, Vietnam. Email: tudn@haui.edu.vn
[b]Institute of International Education, Nguyen Tat Thanh University, Ho Chi Minh City, Vietnam. Email: htnhan@ntt.edu.vn

* Corresponding author

Abstract

This study presents an enhanced finite element method (FEM) integrated with the improved first-order shear deformation theory (i-FSDT) for analyzing the natural frequencies of functionally graded sandwich (FGSW) plates resting on a variable elastic foundation (VEF) with uncertain input parameters. The FGSW plates are composed of two functionally graded (FG) face layers and a homogeneous or FG core layer. The proposed method is validated by comparing it with existing benchmark solutions to ensure its accuracy and reliability. In addition, the study explores the effects of geometric configurations, material properties, foundation types, and boundary conditions (BCs) on the natural frequencies of FGSW plates. To address uncertainty in input parameters, Monte Carlo simulation (MCS) is employed to determine the probabilistic range of natural frequencies. The numerical and graphical results show that the uncertainties of the input parameters interact to greatly affect the natural frequency of sandwich plates.

Keywords

Sandwich plates; Monte Carlo simulation; Q4 element; r-FSDT; Uncertain parameters.

Graphical Abstract

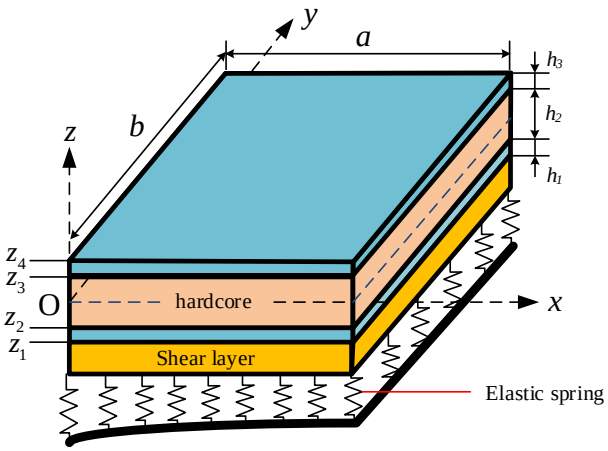

The FGSW plate (Pattern 1)

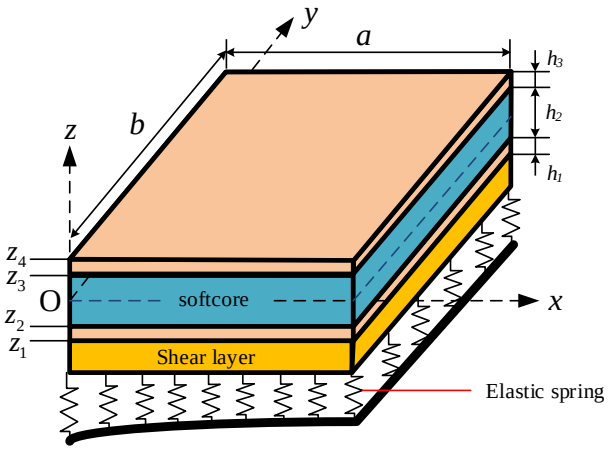

The FGSW plate (Pattern 2)

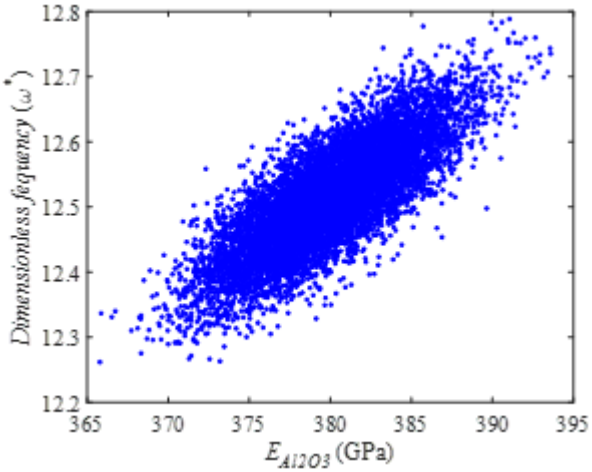

The range of frequency versus uncertain parameter $E_{\mathrm{Al_2O_3}}$

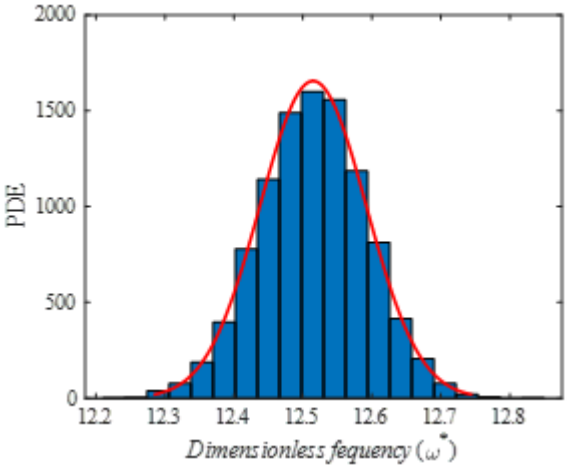

The distribution function of the natural frequency ($Sk_\tau = 0.0273; Ku_\tau = 2.9551$)

1 INTRODUCTION

Sandwich structures are typically constructed of two thin, high-strength laminates with a thick, lightweight core. This design provides exceptional bending stiffness with optimized weight. In addition, sandwich panels also have excellent sound and thermal insulation properties. However, the susceptibility to stress concentrations at load-bearing points and potential weaknesses due to geometric or material inconsistencies are limitations that need to be considered. So, the investigation of their mechanical behavior is necessary and of practical significance in engineering. Several typical deformation theories have been proposed to study sandwich structures, such as the FSDT (Do & Tran, 2024; Hosseini-Hashemi, Taher, Akhavan, & Omidi, 2010; Luat et al., 2021; Thanh, Van Ke, Hoa, & Trung, 2021; Tran & Le, 2023), the higher-order shear deformation theory (HSDT) (J. Reddy, 2000, 2011; Talha & Singh, 2010; H.-T. Thai & Kim, 2013; A. M. Zenkour, 2006, 2013b), *n*th-order shear deformation theory (Yaghoobi & Fereidoon, 2014), or quasi-3D theory (Mantari & Soares, 2013; Neves, Ferreira, Carrera, Cinefra, Roque, et al., 2012; Sobhy & Al Mukahal, 2023), and many refined shear deformation theories.

Several typical works have explored the mechanical behaviors of sandwich plates. For example, A. M. Zenkour (2013a) used an exact solution to analyze the bending of FGSW plates. Zarga (2019) presented an exact method based on quasi-3D theory to examine the thermomechanical bending of FGSW plates. Alibeigloo and Alizadeh (2015) analyzed the frequencies and static problems of FGSW plates using the differential quadrature method (DQM) within the framework of third-order shear deformation theory (TSDT). Natarajan and Manickam (2012) examined the mechanical response of FGSW plates using an efficient quasi-3D theory. Li, Iu, and Kou (2008) applied TSDT to investigate the frequencies of FGSW plates. (Neves et al., 2017; Neves, Ferreira, Carrera, Cinefra, Jorge, et al., 2012) examined the static and buckling of FGSW plates using zigzag theory based on HSDT. Liu and Jeffers (2017) employed layer-wise displacement theory and isogeometric analysis (IGA) to analyze FGSW plates. Additionally, studies on static and dynamic response of sandwich plate can be found in other sources (Neves et al., 2013; Q.-H. Pham, Nguyen, & Tran, 2022; Q.-H. Pham, Tran, & Nguyen, 2023a, 2023b; Q. H. Pham, Tran, Zenkour, & Nguyen-Thoi, 2023; H.-T. Thai, Nguyen, Vo, & Lee, 2014; Tran & Truong Thi Huong, 2024; Tran, Zenkour, & Pham, 2025; A. Zenkour, 2005).

In the last few years, there has been a growing interest among researchers in exploring plates and shells supported by elastic foundations (EF). Commonly used foundation models in such studies include the Winkler Foundation (WF), a one-parameter model (Katsikadelis & Armenakas, 1984); Pasternak Foundation (PF), a two-parameter model (Avcar & Mohammed, 2018); and Kerr Foundation (KF), a three-parameter model (Keshtegar, Motezaker, Kolahchi, & Trung, 2020). Among these, the two-parameter Pasternak model is frequently employed, while the Kerr model can be reduced to the other two foundation models. Several authors have concentrated on examining the mechanical response of structures supported by EFs, including (Tounsi et al., 2024; Tounsi, Mostefa, Attia, et al., 2023; Tounsi, Mostefa, Bousahla, et al., 2023), (Belabed, Bousahla, Houari, Tounsi, & Mahmoud, 2018; Belabed, Tounsi, Al-Osta, Tounsi, & Minh, 2024), Bounouara et al. (2023), Gawah et al. (2024), and Lafi et al. (2024). Moreover, additional numerical results related to the mechanical behavior analysis of structures resting on EFs can be found in references (Bouadi, Bousahla, Houari, Heireche, & Tounsi, 2018; Do, Nguyen, Tran, Le, & Pham, 2023; Le, Tran, Pham, & Pham, 2025; Mudhaffar et al., 2023; T. T. Nguyen, Le, Tran, & Pham, 2024; V. C. Nguyen, Tran, Sobhy, Hoang, & Hoa Pham, 2025; Q.-H. Pham et al., 2023b; Tran & Truong Thi Huong, 2024; Tran et al., 2025).

The FEM was first introduced by Clough (1960). This method involves discretizing the problem domain into smaller, geometrically simpler components known as "finite elements". Within each element, displacement variables are represented using shape functions. The accuracy of structural analysis using FEM improves with higher-order shape functions. However, employing higher-order shape functions also introduces mathematical complexity. Today, FEM is widely used in structural analysis and offers significant advantages over analytical methods, particularly for structures with complex geometries and arbitrary boundary conditions (Akbaba, Yıldırım, & Canbaloğlu, 2022; V. C. Nguyen, Tran, Nguyen-Thoi, & Pham, 2022; Uddin, Rasel, Adewole, & Al Kalbani, 2022; Vu, Pham, Tran, & Pham, 2023).

Although the use of a four-node element (so-called Q4 element) has been a convenient and effective method for analyzing the mechanical behavior of structures, yielding promising preliminary results, it becomes evident that relying on only five degrees of freedom (DOFs) per node-based on Lagrange interpolations with a shear correction factor-fails to fully satisfy the stress-free conditions at the upper and lower surfaces of plates. To address this issue, several methods have been proposed, including IGA (C. H. Thai, Nguyen-Xuan, & Phung-

Van, 2023), an exact solution based on HSDT (Djilali et al., 2022), FEM combined with TSDT based on Hermite and Lagrange approximations (Do & Pham, 2023), and others. Although these methods offer high accuracy, their complex mathematical formulations and/or the increased number of DOFs lead to higher computational costs, particularly when combined with MCS for uncertain natural frequency analysis. To address these constraints, our work employs i-FSDT.

In traditional analysis, it is often assumed that the input parameters are deterministic. However, because of random differences in construction, manufacturing methods, aging, and operational circumstances, these parameters are frequently unclear and are best described by probability density functions (PDFs). As a result, state functions that represent design conditions cannot be determined with certainty by employing deterministic design methods. The stochastic design technique revolves around evaluating the state function within the context of the PDF for uncertain parameters (Kapur & Lamberson, 1977; Smith, 2024). These methods provide insights into structural natural frequencies and allow reliability-based design improvement.

The mechanical behavior of composite structures has garnered significant attention from scientists worldwide. Despite the numerous advantages of composite structures, a key drawback is the occurrence of delamination and the discontinuity of transverse shear stress along the plate's thickness. A sandwich structure, a type of composite structure, features a thick, lightweight core layer protected by two outer skin layers that are highly durable and heat-resistant. This combination of material layers ensures the continuity of shear stress through the plate's thickness. The primary goal of this study is to develop an enhanced FEM based on the classical Q4 element for analyzing FGSW plates supported by VEF. After validating the accuracy and performance of the proposed elements, this work also examines the impact of geometric parameters, material properties, type of foundations, and BCs on the natural frequency of FGSW plates supported by the VEF. Additionally, the natural frequency of FGSW plates under uncertain input parameters is fully explored.

2 THEORETICAL FORMULATION

2.1 The FGSW plate model

Considering rectangular FGSW plates with a hardcore (Pattern 1) and a softcore (Pattern 2), as shown in Figure 1. The group of $h_1 - h_2 - h_3$ represents the thickness ratios of the bottom, the core, and the top layer of plates (also referred to as the "scheme"); $h = h_1 + h_2 + h_3$ is the total thickness of the plate.

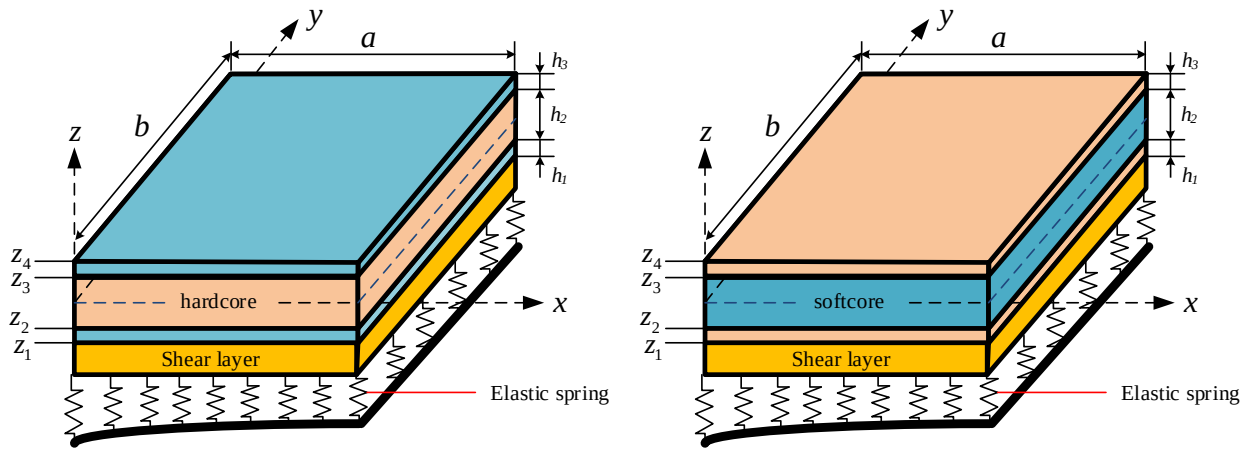

a) The FGSW plate (Pattern 1). b) The FGSW plate (Pattern 2).

Figure 1 The FGSW plate model placed on the VEF.

The volume $V_c^{(i)}$ of the ceramic phase of each layer is determined by Akavci (2016):

+ For Pattern 1:

$$\begin{cases} V_c^{(1)} = \left(\dfrac{z - z_1}{z_2 - z_1}\right)^k & z \in [z_1; z_2] \\ V_c^{(2)} = 1 & z \in (z_2; z_3) \\ V_c^{(3)} = \left(\dfrac{z - z_4}{z_3 - z_4}\right)^k & z \in [z_3; z_4] \end{cases} \quad (1a)$$

+ For Pattern 2:

$$\begin{cases} V_c^{(1)} = 1 - \left(\dfrac{z - z_1}{z_2 - z_1}\right)^k & z \in [z_1; z_2] \\ V_c^{(2)} = 0 & z \in (z_2; z_3) \\ V_c^{(3)} = 1 - \left(\dfrac{z - z_4}{z_3 - z_4}\right)^k & z \in [z_3; z_4] \end{cases} \tag{1b}$$

The effective material properties of FGSW plates are determined by

$$P^{(i)}(z) = P_c V_c^{(i)} + P_m\left(1 - V_c^{(i)}\right), \quad i = 1,2,3 \tag{2}$$

here, $P^{(i)}(z)$ represents the material characteristics of each layer, such as Young's modulus, Poisson's ratio, and mass density; k is the power-law index. Additionally, Figure 2 shows the plot of the effective Young's modulus versus the thickness of the FGSW (Al/Al_2O_3) plate (1-2-1) with the mechanical properties provided in Table 1.

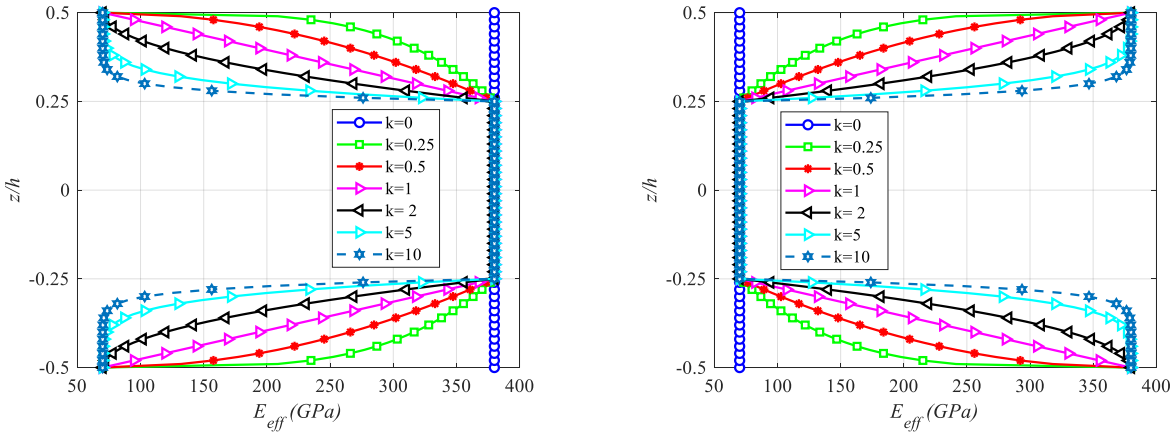

a) Pattern 1 b) Pattern 2

Figure 2 The effective Young's modulus via the FGSW plate thickness (scheme 1-2-1).

Table 1 The mechanical properties of component materials.

Materials	Young's modulus (GPa)	Density (kg/m3)	Poisson's ratio
Al_2O_3	380	3800	0.3
ZrO_2	151	3000	0.3
Al	70	2707	0.3

2.2 The VEF model

In reality, the elastic foundation (EF) is not uniform and does not provide uniform support across the plate. In this study, we employ three heterogeneous foundation models to represent the non-uniform support of EFs better and more realistically. These foundation models ensure continuity, satisfying integrability conditions when calculating foundation stiffness matrices. The plate is considered to rest on the PF model, as specified by Keshtegar et al. (2020):

$$\mathbb{R} = k_1 w - k_2\left(\frac{\partial^2 w}{\partial x^2} + \frac{\partial^2 w}{\partial y^2}\right) \tag{3}$$

where $\mathbb{R}$ represents the reaction force of the EF, and k_1 is the Winkler parameter, which is dependent on *x*-axis only. It is assumed to have a linear, parabolic, or sinusoidal variation, given by Pradhan and Murmu (2009):

$$k_1 = \frac{K_1 h^3}{a^4}\begin{cases} 1 + \mu\dfrac{x}{a} & linear \quad \text{(Type 1)} \\ 1 + \mu\left(\dfrac{x}{a}\right)^2 & parabolic \quad \text{(Type 2)} \\ 1 + \mu sin\left(\dfrac{\pi x}{a}\right) & sinusoidal \quad \text{(Type 3)} \end{cases} \tag{4}$$

where K_1 is a constant and μ is a variable parameter, k_2 denotes the shear layer stiffness. Notably, when μ is zero, the VEF simplifies to the PF.

2.3 The r-FSDT

According to the FSDT, the displacement of any point on FGSW plates is defined by J. N. Reddy (2003):

$$\begin{cases} u(x,y,z) = u_0(x,y) + z\theta_x(x,y) \\ v(x,y,z) = v_0(x,y) + z\theta_y(x,y) \\ w(x,y,z) = w_0(x,y) \end{cases} \tag{5}$$

where u_0, v_0, w_0, θ_x, θ_y are the displacement variables in the mid-plane of plates (see Fig. 3).

The normal strain is represented by

$$\boldsymbol{\varepsilon} = \boldsymbol{\varepsilon}_m + z\boldsymbol{\kappa}, \tag{6}$$

in which

The membrane strain as

$$\boldsymbol{\varepsilon}_m = \begin{Bmatrix} u_{0,x} \\ v_{0,y} \\ u_{0,y} + v_{0,x} \end{Bmatrix}. \tag{7}$$

The bending strain as

$$\boldsymbol{\kappa} = \begin{Bmatrix} \theta_{x,x} \\ \theta_{y,y} \\ \theta_{x,y} + \theta_{y,x} \end{Bmatrix}. \tag{8}$$

The transverse shear strain as

$$\boldsymbol{\gamma} = g(z)\begin{Bmatrix} w_{0,x} + \theta_x \\ w_{0,y} + \theta_y \end{Bmatrix}, \tag{9}$$

with $g(z)$ is introduced by H. N. Nguyen, Hong, Vinh, Quang, and Thom (2019):

$$g(z) = \frac{5}{4}\cos\left(\frac{\pi z}{h}\right). \tag{10}$$

The stress-strain relationships based on Hooke's law by J. N. Reddy (2003):

$$\begin{Bmatrix} \sigma_x \\ \sigma_y \\ \tau_{xy} \\ \tau_{xz} \\ \tau_{yz} \end{Bmatrix} = \begin{bmatrix} Q_{11} & Q_{12} & 0 & 0 & 0 \\ Q_{21} & Q_{22} & 0 & 0 & 0 \\ 0 & 0 & Q_{66} & 0 & 0 \\ 0 & 0 & 0 & Q_{55} & 0 \\ 0 & 0 & 0 & 0 & Q_{44} \end{bmatrix} \begin{Bmatrix} \varepsilon_x \\ \varepsilon_y \\ \gamma_{xy} \\ \gamma_{xz} \\ \gamma_{yz} \end{Bmatrix}, \tag{11}$$

where

$$Q_{11} = Q_{22} = \frac{E(z)}{1-\upsilon^2}, \quad Q_{12} = Q_{21} = \frac{\upsilon E(z)}{1-\upsilon^2}, Q_{44} = Q_{55} = Q_{66} = \frac{E(z)}{2(1+\upsilon)}. \tag{12}$$

The i-FSDT is chosen as a practical compromise; it significantly improves accuracy over classical FSDT and satisfies the condition that the shear stress is curvilinear and zero at the top and bottom surfaces of the plate while avoiding the complexity and computational burden of HSDT, making it suitable for many real-world structural analyses, especially when combined with MCS.

2.4 Weak form of FGSW plates

Using Hamilton's principle, the governing equations for plates are determined by J. N. Reddy (2003):

$$\int_{t_1}^{t_2}\left(\delta\mathcal{U} + \delta U^f - \delta\mathcal{K}\right)\mathrm{d}t = 0, \tag{13}$$

where

The strain energy $\mathcal{U}$ as

$$\mathcal{U} = \frac{1}{2}\int_{\psi}\left(\boldsymbol{\varepsilon}^T\boldsymbol{D}\boldsymbol{\varepsilon} + \boldsymbol{\gamma}^T\mathbb{A}_p\boldsymbol{\gamma}\right)\mathrm{d}\psi, \tag{14}$$

with

$$\boldsymbol{\varepsilon} = [\boldsymbol{\varepsilon}_m \quad \boldsymbol{\kappa}]^T, \quad \boldsymbol{D} = \begin{bmatrix} \mathbb{A} & \mathbb{B} \\ \mathbb{B} & \mathbb{C} \end{bmatrix}, \tag{15}$$

and $\mathbb{A}$, $\mathbb{B}$, $\mathbb{C}$, and $\mathbb{A}_p$ are calculated by

$$(\mathbb{A},\mathbb{B},\mathbb{C}) = \int_{-h/2}^{h/2}(1,z,z^2)\begin{bmatrix} Q_{11} & Q_{12} & 0 \\ Q_{21} & Q_{22} & 0 \\ 0 & 0 & Q_{66} \end{bmatrix}\mathrm{d}z, \tag{16}$$

$$\mathbb{A}_p = \int_{-h/2}^{h/2} g(z)\begin{bmatrix} Q_{55} & 0 \\ 0 & Q_{44} \end{bmatrix}\mathrm{d}z. \tag{17}$$

The foundation's strain energy U^f as

$$U^f = \frac{1}{2}\int_{\psi} \left(k_1 w^2 + k_2\left(w_{,x}^2 + w_{,y}^2\right)\right) \mathrm{d}\psi \tag{18}$$

The kinetic energy of the plate $\mathcal{K}$ as

$$\mathcal{K} = \frac{1}{2}\int_{\psi} \dot{\boldsymbol{u}}^T \mathbb{M} \dot{\boldsymbol{u}} \mathrm{d}\psi. \tag{19}$$

in which $\boldsymbol{u}^T = [u_0 \quad v_0 \quad w_0 \quad \theta_x \quad \theta_y]$, and $\mathbb{M}$ is the mass matrix determined by

$$\mathbb{M} = \begin{bmatrix} m_1 & 0 & 0 & m_2 & 0 \\ & m_1 & 0 & 0 & m_2 \\ & & m_1 & 0 & 0 \\ & & & m_3 & 0 \\ \text{sym} & & & & m_3 \end{bmatrix}, \tag{20}$$

with $\{m_1, m_2, m_3\} = \int_{-h/2}^{h/2} \rho(z)\{1, z, z^2\}\mathrm{d}z$.

Replacing Eq. (14), Eqs. (18)-(19) into Eq. (13), the weak form of FGSW plates is defined by

$$\int_{\psi} \delta\boldsymbol{\varepsilon}^T \boldsymbol{D} \boldsymbol{\varepsilon} \mathrm{d}\psi + \int_{\psi} \delta\boldsymbol{\gamma}^T \mathbb{A}_p \boldsymbol{\gamma} \mathrm{d}\psi + \int_{\psi} \mathbb{R}\delta\boldsymbol{w}\, \mathrm{d}\psi = \int_{\psi} \boldsymbol{u}^T \mathbb{M} \ddot{\boldsymbol{u}} \mathrm{d}\psi. \tag{21}$$

2.5 Finite element procedure

In this article, the Q4 element with 5 DOFs per node offers a good balance of accuracy, computational efficiency, and compatibility with advanced plate theories, making it a reliable choice for the structural analysis of plates. The element displacement vector is introduced by

$$\boldsymbol{q}_e = [\boldsymbol{q}_1^T \quad \boldsymbol{q}_2^T \quad \boldsymbol{q}_3^T \quad \boldsymbol{q}_4^T]^T, \tag{22}$$

with the node displacement vector is shown in Figure 3 by Ferreira (2009):

$$\boldsymbol{q}_i = \{u_{0i} \quad v_{0i} \quad w_i \quad \theta_{xi} \quad \theta_{yi}\} \qquad i = 1,2,3,4. \tag{23}$$

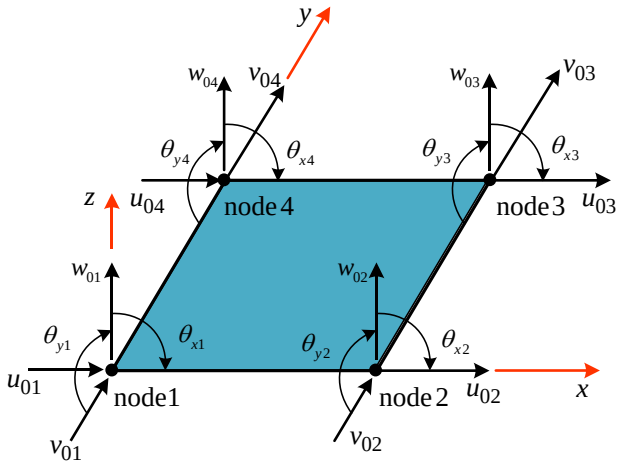

Figure 3 The Q4 element model with five DOFs.

Replacing Eq. (22) into Eq. (4), the strain vectors can be determined by

$$\boldsymbol{\varepsilon} = [\mathbf{B}_1 \quad \mathbf{B}_2]\boldsymbol{q}_e, \tag{24a}$$

$$\boldsymbol{\gamma} = \mathbf{B}_3 \boldsymbol{q}_e, \tag{24b}$$

with

$$\mathbf{B}_1 = \sum_{i=1}^{4} \begin{bmatrix} N_{i,x} & 0 & 0 & 0 & 0 \\ 0 & N_{i,y} & 0 & 0 & 0 \\ N_{i,y} & N_{i,x} & 0 & 0 & 0 \end{bmatrix}, \tag{25a}$$

$$\mathbf{B}_2 = \sum_{i=1}^{4} \begin{bmatrix} 0 & 0 & N_{i,x} & 0 & 0 \\ 0 & 0 & 0 & N_{i,y} & 0 \\ 0 & 0 & N_{i,y} & N_{i,x} & 0 \end{bmatrix}, \tag{25b}$$

and

$$\mathbf{B}_3 = \sum_{i=1}^{4} \begin{bmatrix} 0 & 0 & N_{i,y} & 0 & N_i \\ 0 & 0 & N_{i,x} & N_i & 0 \end{bmatrix}. \tag{25c}$$

Now, the vibration equation of the plate element as

$$\boldsymbol{M}_e \ddot{\boldsymbol{q}}_e + (\boldsymbol{K}_e + \boldsymbol{K}_e^f)\boldsymbol{q}_e = \boldsymbol{0} \tag{26}$$

where

The element stiffness matrix $\boldsymbol{K}_e$ as

$$\boldsymbol{K}_e = \int_{\psi} \left(\begin{Bmatrix} \boldsymbol{B}_1 \\ \boldsymbol{B}_2 \\ \boldsymbol{B}_3 \end{Bmatrix}^T \begin{bmatrix} \mathbb{A} & \mathbb{B} & 0 \\ \mathbb{B} & \mathbb{C} & 0 \\ 0 & 0 & \mathbb{A}_p \end{bmatrix} \begin{Bmatrix} \boldsymbol{B}_1 \\ \boldsymbol{B}_2 \\ \boldsymbol{B}_3 \end{Bmatrix} \right) \mathrm{d}\psi. \tag{27}$$

The foundation element stiffness matrix $\boldsymbol{K}_e^f$ as

$$\boldsymbol{K}_e^f = k_1 \int_{\psi} \mathbf{N}_w^{\mathrm{T}} \mathbf{N}_w \, \mathrm{d}\psi + \mathrm{k}_2 \int_{\psi} \left[\left(\frac{\partial \mathbf{N}_w}{\partial \mathrm{x}} \right)^{\mathrm{T}} \left(\frac{\partial \mathbf{N}_w}{\partial \mathrm{x}} \right) + \left(\frac{\partial \mathbf{N}_w}{\partial \mathrm{y}} \right)^{\mathrm{T}} \left(\frac{\partial \mathbf{N}_w}{\partial \mathrm{y}} \right) \right] \mathrm{d}\psi \tag{28}$$

The element mass matrix $\boldsymbol{M}_e$ as

$$\boldsymbol{M}_e = \int_{\psi} \boldsymbol{N}^T \mathbb{M} \boldsymbol{N} \, \mathrm{d}\psi, \tag{29}$$

in which $\boldsymbol{N}$ is the shape function matrix defined by

$$\boldsymbol{N} = \sum_{i=1}^{4} \begin{bmatrix} N_i & 0 & 0 & 0 & 0 \\ & N_i & 0 & 0 & 0 \\ & & N_i & 0 & 0 \\ & & & N_i & 0 \\ \mathrm{sym} & & & & N_i \end{bmatrix}. \tag{30}$$

Then, the governing equation of the FGSW plate as

$$\boldsymbol{M}\ddot{\boldsymbol{q}} + (\boldsymbol{K} + \boldsymbol{K}^f)\boldsymbol{q} = \boldsymbol{0} \tag{31}$$

herein, $\boldsymbol{K} = \sum_{nel} \boldsymbol{K}_e$, $\boldsymbol{M} = \sum_{nel} \boldsymbol{M}_e$ and $\boldsymbol{K}^f = \sum_{nel} \boldsymbol{K}_e^f$ denote the global stiffness matrix, the global mass matrix and the global foundation stiffness matrix, respectively. These global matrices are assembled from element matrices based on the index matrix of the finite element algorithm (Ferreira, 2009), with "*nel*" being the total number of elements.

The assumption that $\boldsymbol{q} = \boldsymbol{q}_0 \sin(\omega t) \neq 0$, we get:

$$\left| \boldsymbol{K} + \boldsymbol{K}^f - \omega^2 \boldsymbol{M} \right| = \boldsymbol{0}, \tag{32}$$

with ω is the natural frequency.

In this study, a Dirichlet boundary condition is applied by imposing displacement constraints along the plate edges (see Figure 4). This condition is commonly used in FEM simulations due to its simplicity and efficiency, allowing flexible imposition of boundary conditions without the need to resolve the problem from scratch as in analytical methods.

- Simply supported (S):

$u_0 = w_0 = \theta_x = 0$ at $y = 0$ & $y = b$ and/or $v_0 = w_0 = \theta_y = 0$ at $x = 0$ & $x = a$.

- Clamped (C):

$u_0 = v_0 = w_0 = \theta_x = \theta_y = 0$.

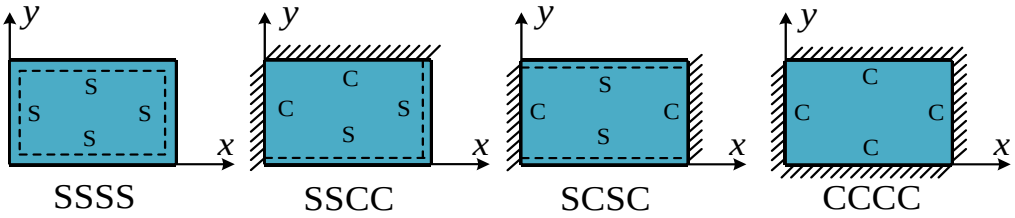

Figure 4 The type of BCs of FGSW plates.

2.6 The uncertain input parameters

In the conventional design approach, design parameters such as load (**L**) and strength (**S**) are considered distinct and predictable values. The relationship between **L** and **S** is fully understood as the design condition, which includes system parameters like frequency. A system is considered secure when its load capacity significantly exceeds the applied load (Do & Tran, 2024; Q.-H. Pham et al., 2023b). However, in real-world situations, these parameters usually behave as uncertain variables, following distribution patterns shown in Figure 5a. Even with traditional safety-focused design principles, there are still vulnerable zones (indicated by the slashed section), where the strength parameter value is lower than that of the load parameter. Additionally, the shape of the dangerous region is influenced by the distribution forms. This critical region can be more easily quantified and managed using reliability theory. This approach involves calculating the system's failure probability by analyzing the distribution of the state function **G** (**G=S-L**). The function **G** depends on the

distribution of the parameters **S** and **L**. A failure occurs when $\mathbf{G} < 0$, while no failure is observed when $\mathbf{G} \geq 0$ (see Figure 5b).

In this work, the uncertain variables include Young's modulus E_{Al}, E_{Al2O3}; mass densities ρ_{Al}, ρ_{Al2O3}; and power-law index k; and indicated by the vector $\boldsymbol{\xi} = [\xi_i]_{i=1:n} = [E_{Al} \quad E_{Al2O3} \quad \rho_{Al} \quad \rho_{Al2O3} \quad k]$ with n is the total number of uncertain variables. The uncertain variables ξ_i are independent and follow a standard distribution with a mean $\bar{\xi}_i$ and uncertain parameter γ_i.

$$\xi_i = \bar{\xi}_i(1 + \gamma_i), \tag{33}$$

here γ_i is described by the mean $\overline{\gamma_i}$ and the standard deviation σ_{γ_i}.

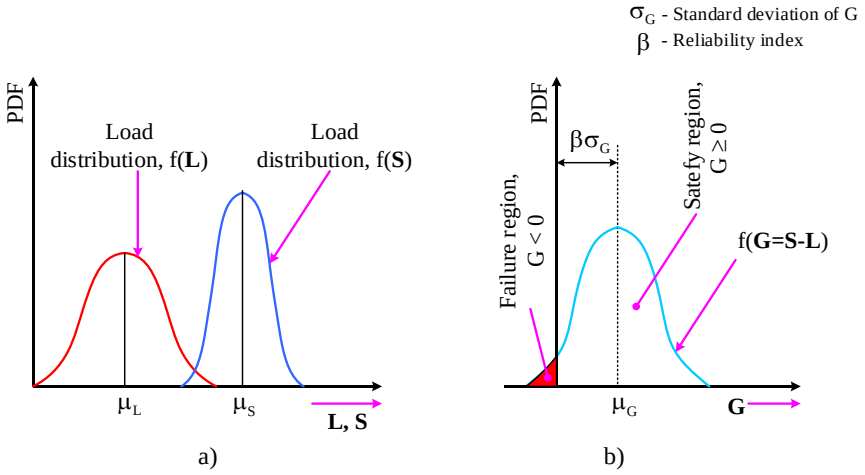

Figure 5 The PDF in uncertain variables.

The characteristics of the uncertain natural frequency are defined by Q.-H. Pham et al. (2023b):

$$\bar{\tau} = \frac{1}{N_s}\sum_{i=1}^{N_s}\tau_i, \quad \sigma_\tau = \sqrt{\frac{1}{N_s-1}\sum_{i=1}^{N_s}(\tau_i - \bar{\tau})^2}, Sk_\tau = \frac{1}{N_s}\sum_{i=1}^{N_s}\left(\frac{\tau_i-\bar{\tau}}{\sigma_\tau}\right)^3, \quad Ku_\tau = \frac{1}{N_s}\sum_{i=1}^{N_s}\left(\frac{\tau_i-\bar{\tau}}{\sigma_\tau}\right)^4. \tag{34}$$

here, N_s is the sample size, $\bar{\tau}$ is the mean; σ_τ is the standard deviation; Sk_τ is the skewness and Ku_τ is the kurtosis of the distribution.

Note that MCS is a flexible and easy-to-implement method for structural analysis when input parameters are uncertain. It can handle complex, nonlinear models and does not require analytical solutions. However, its main drawback is the high computational cost, as a large number of simulations are needed to achieve accurate results, especially for rare event estimation. Therefore, MCS is well-suited for general probabilistic assessments but may be inefficient for problems requiring fast computation or very low failure probability estimation.

3 VERIFICATION AND RESULTS NUMBER

In this section, we created a MATLAB program to do the computations with MATLAB version R2018a. The computations were carried out using a laptop running Windows 10 Pro and equipped with an Intel(R) Core(TM) i5-4300M CPU @ 2.60GHz and 8.0 GB of RAM. The dimensionless parameters are given as

$$\omega^* = \omega\frac{a^2}{h_0}\sqrt{\frac{\rho_0}{E_0}}; \rho_0 = 1kg/m^3; K_1 = k_1\frac{a^4}{D_c}; \; K_2 = k_2\frac{a^2}{D_c} \text{ with } D_c = \frac{E_{Al2O3}{h_0}^3}{12(1-\nu_{Al2O3}^2)} \tag{35}$$

3.1 Verification studies

Example 1: Considering the SSSS square FG (Al/Al_2O_3) plate placed on EF. The dimensionless frequency is provided by $\omega^{**} = \omega h\sqrt{\frac{\rho_{Al}}{E_{Al}}}$. Observing that the obtained results converge at a mesh size of 14×14 and well agree with those of exact methods employing quasi-3D (Shahsavari, Shahsavari, Li, & Karami, 2018) and TSDT (Baferani, Saidi, & Ehteshami, 2011), as given in Table 2 and displayed in Figure 6. However, to ensure accuracy and achieve high smoothness of the deformation field, the mesh size of 16×16 is used for the following studies.

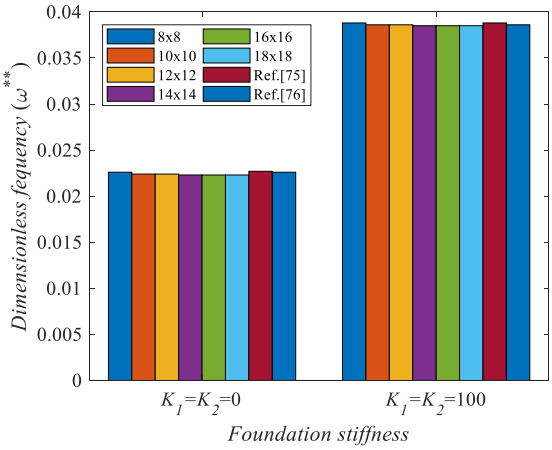

Figure 6 Convergence of the proposed element.

Table 2 The dimensionless frequencies ω^{**} of FG (Al/Al_2O_3) plates placed on EF with k=1 and $h = a/20$.

(K_1, K_2)	Method	Meshing					
		8×8	10×10	12×12	14×14	16×16	18×18
(0,0)	Present	0.0226	0.0224	0.0224	0.0223	0.0223	0.0223
	Shahsavari et al. (2018)			0.0227			
	Baferani et al. (2011)			0.0226			
(100,100)	Present	0.0388	0.0386	0.0386	0.0385	0.0385	0.0385
	Shahsavari et al. (2018)			0.0388			
	Baferani et al. (2011)			0.0386			

Example 2: We examine the SSSS FGSW (Al/ZrO_2) plate placed on EF, considering both thin ($a/h = 100$) and moderately thick ($a/h = 10$) configurations. The dimensionless frequencies $\omega^* = \omega \frac{a^2}{h}\sqrt{\frac{\rho_0}{E_0}}$ with ($\rho_0 = 1kg/m^3, E_0 = 1GPa$) are provided in Table 3. It is evident that the results obtained are in full agreement with those of Akavci (2016), who used an exact solution based on the hyperbolic shear deformation theory.

Table 3 The frequencies ω^* of FGSW plates placed on EF.

a/h	k	Scheme	Foundation stiffness					
			$(0,0)$		$(10,10)$		$(100,100)$	
			Present	Akavci (2016)	Present	Akavci (2016)	Present	Akavci (2016)
10	0	2-1-2	1.29798	1.29692	1.62162	1.61603	3.33662	3.31161
		1-1-1	1.29798	1.29692	1.62162	1.61603	3.33662	3.31161
		2-2-1	1.29798	1.29692	1.62162	1.61603	3.33662	3.31161
	2	2-1-2	0.99494	0.99389	1.40948	1.40287	3.31005	3.28172
		1-1-1	1.01906	1.01785	1.42350	1.41684	3.30402	3.27584
		2-2-1	1.04322	1.04293	1.43930	1.43347	3.30460	3.27742
	10	2-1-2	0.93809	0.93742	1.3774	1.37067	3.32436	3.29462
		1-1-1	0.95353	0.95372	1.38365	1.37733	3.31076	3.28050
		2-2-1	0.97969	0.98239	1.39945	1.39522	3.30840	3.28023
100	0	2-1-2	1.34539	1.34038	1.66396	1.65899	3.37595	3.36942
		1-1-1	1.34539	1.34038	1.66396	1.65899	3.37595	3.36942
		2-2-1	1.34539	1.34038	1.66396	1.65899	3.37595	3.36942
	2	2-1-2	1.02204	1.01820	1.43385	1.43000	3.34037	3.33441
		1-1-1	1.04663	1.04279	1.44837	1.44444	3.33449	3.32829
		2-2-1	1.0722	1.06946	1.46539	1.46227	3.33575	3.32997

10	2-1-2	0.96421	0.96023	1.40068	1.39670	3.35438	3.34801
	1-1-1	0.97871	0.97582	1.40639	1.40285	3.34041	3.33315
	2-2-1	1.00607	1.00620	1.42325	1.42192	3.33868	3.33266

3.2 Natural frequency analysis with deterministic parameters

Firstly, the first six eigenmodes of FGSW (Al/Al_2O_3) plates in three types of VEFs with Pattern 1 are plotted in Figure 7 and with Pattern 2 as shown in Figure 8. It can be observed that the deformation in each case is asymmetrical, depending on the support by the type of EFs and BCs. Generally, the greatest deformation occurs in the area of sandwich plates that is less supported by the foundation. As shown in Figure 9, for each Pattern, the sandwich plate supported by Type 3 results in the largest natural frequency, followed by Type 2 and the smallest by Type 1. In addition, for each foundation style, there will be equal natural frequency pairs, i.e., the same eigenmode, but only different in viewing direction. Besides, the sandwich plate with Pattern 2 results in the first frequency being larger than that of Pattern 1, however, the opposite happens with the higher frequencies, i.e., the higher frequencies of the FGSW plate of Pattern 1 will be larger than that of Pattern 2. It can be seen that the natural frequency of FGSW plates depends simultaneously on both the overall stiffness and the overall mass of the sandwich plates as well as the elastic foundation stiffness, so it is necessary to study the influence of the schemes, power-law index, foundation types, and Patterns on the natural frequency of FGSW plates.

Secondly, Table 4 and Figure 10 provide the natural frequency of the FGSW plates when the input parameters are varied. It can be seen that, with Pattern 1 (hardcore), the thicker the ceramic defect, the lower the natural frequency corresponding to the schemes 2-1-2, 1-2-2,1-2-1, 1-4-1, and 1-0-1. Although the ceramic core thickness increases, the sandwich plate becomes stiffer, but the mass of the sandwich plate also increases faster, so the natural frequency decreases. In addition, as the power-law index increases, the oscillation frequency also increases. This is because increasing *k* leads to a decrease in the stiffness of plates, but the mass decreases even faster. With Pattern 2 (softcore), the natural frequency changes with a more complex rule. Specifically, the thicker the metal core, the higher the natural frequency corresponds to diagrams 2-1-2, 1-2-2, 1-2-1, 1-4-1 and 1-0-1. Increasing *k* results in a decrease in the natural frequency of schemes 1-0-1, 2-1-2, and 1-2-2 supported by Type 1; and the scheme 1-0-1 of Type 2 and Type 3. As k increases, the natural frequency of plates increases, corresponding to the schemes 2-1-2, 1-2-2, 1-2-1, and 1-4-1 (except *k*=1) supported by Type 2 and Type 3. In the remaining cases, *k*=1 results in the maximum frequency.

Moreover, Table 5 and Table 6 list the first six natural frequencies corresponding to different input parameters and BCs for the two Patterns. It can be seen that the frequencies increase respectively with the SSSS, SSCC, SCSC, and CCCC, as expected.

3.3 Natural frequency analysis with uncertain parameters

In this examination, the authors assume that uncertain quantities have the same standard deviation at different levels $\sigma_\gamma = 0.01; 0.1$. The average value of the input uncertain parameters $\bar{\xi}_i$ is obtained as the deterministic values listed in Table 1, i.e.: $\bar{E}_{Al} = 70$ GPa; $\bar{E}_{\mathrm{Al_2O_3}} = 380$ GPa; $\bar{\rho}_{\mathrm{Al}} = 2707\ \mathrm{kg/m^3}$; $\bar{\rho}_{\mathrm{Al_2O_3}} = 3800\ \mathrm{kg/m^3}$, and $\bar{k} = 1$. Figure 11 presents the PDF of the uncertain variable $E_{\mathrm{Al_2O_3}}$ whose width increases with increasing standard deviation. To account for the uncertainty in design parameters and determine the natural frequency of FGSW plates, a sampling size of $N_s = 10^4$ is employed.

Figure 12 illustrates the variation range of the natural frequency of FGSW plates corresponding to standard deviations $\sigma_\gamma = 0.03$ and 0.1 under uncertain input parameters listed in Table 7. It is observed that the frequency range associated with the uncertain parameters $E_{\mathrm{Al_2O_3}}$ and $\rho_{\mathrm{Al_2O_3}}$ forms a circular distribution, while the range for E_{Al}, and k appears elliptical. In contrast, the variation due to ρ_{Al} results in a nearly circular shape. These results indicate that uncertainties of $E_{\mathrm{Al_2O_3}}$ and $\rho_{\mathrm{Al_2O_3}}$ have a more significant impact on the natural frequency compared to ρ_{Al}, E_{Al} and k. Furthermore, the distribution of the natural frequency (with skewness $Sk_\tau = 0.0273$ and kurtosis $Ku_\tau = 2.9551$) closely resembles a standard distribution, as shown in Figure 12f. It is noteworthy that a skewness of zero and a kurtosis of three correspond to a mesokurtic (standard) distribution.

Finally, Table 8 and Figure 13 illustrate the impact of the standard deviation σ_γ on the probability distribution function of the natural frequency of the FGSW plate. As expected, an increase in σ_γ results in a corresponding increase in the skewness Sk_τ of the distribution. A negative skewness value indicates a left-

skewed leptokurtic distribution, whereas a positive skewness implies a right-skewed leptokurtic distribution. When σ_γ is less than 0.1, the Ku_τ in all cases remains close to 3, which is consistent with that of a standard normal distribution. Kurtosis is a statistical measure that reflects the propensity of a distribution to produce outliers. A kurtosis value greater than 3 indicates a distribution that is more prone to outliers (leptokurtic), while a value less than 3 suggests a distribution with fewer outliers (platykurtic).

Foundation types	The eigenmodes					
	1st mode	2nd mode	3rd mode	4th mode	5th mode	6th mode
Type 1	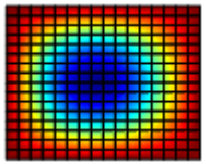	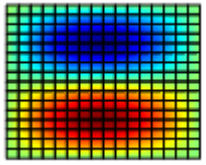	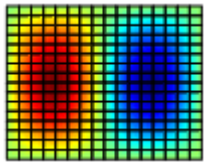	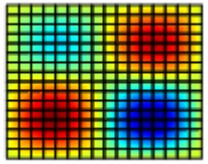	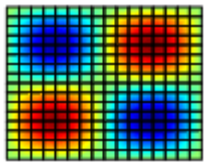	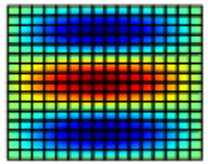
	$\omega_1^* = 2.5531$	$\omega_2^* = 4.3703$	$\omega_3^* = 4.3785$	$\omega_4^* = 5.8132$	$\omega_5^* = 5.8132$	$\omega_6^* = 6.2721$
Type 2	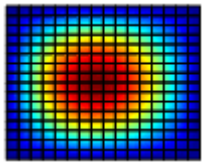	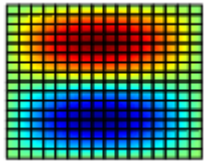	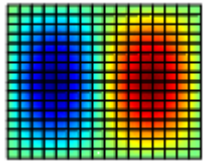	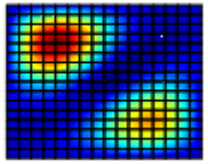	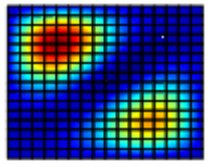	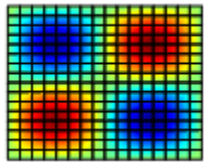
	$\omega_1^* = 2.3404$	$\omega_2^* = 4.2516$	$\omega_3^* = 4.2809$	$\omega_4^* = 5.8132$	$\omega_5^* = 5.8132$	$\omega_6^* = 6.2053$
Type 3	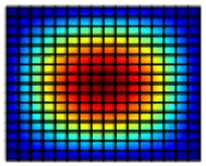	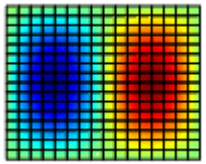	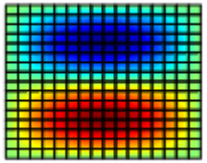	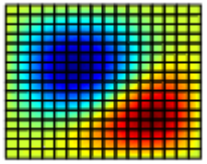	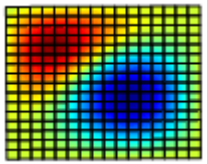	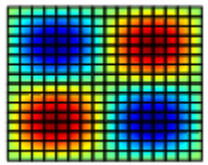
	$\omega_1^* = 2.8697$	$\omega_2^* = 4.4689$	$\omega_3^* = 4.5572$	$\omega_4^* = 5.8132$	$\omega_5^* = 5.8132$	$\omega_6^* = 6.3361$

Figure 7 The first six eigenmodes of FGSW plates (SSSS, $/b = 1, a/h = 10, K_1 = 100, K_2 = 5, \mu = 5$, $k = 1$, scheme 1-3-1, and Pattern 1).

Foundation types	The eigenmodes					
	1st mode	2nd mode	3rd mode	4th mode	5th mode	6th mode
Type 1	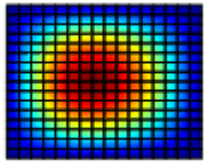	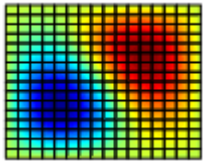	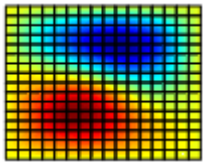	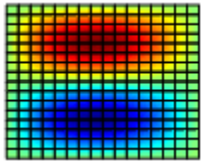	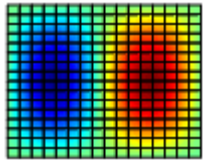	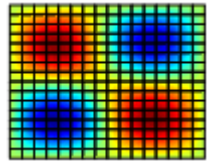
	$\omega_1^* = 2.7240$	$\omega_2^* = 4.1488$	$\omega_3^* = 4.1488$	$\omega_4^* = 4.3425$	$\omega_5^* = 4.3564$	$\omega_6^* = 5.8761$
Type 2	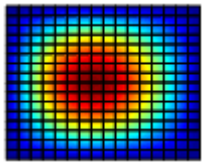	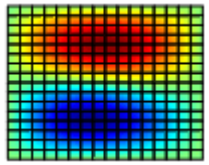	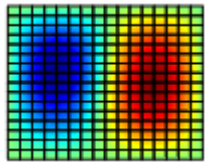	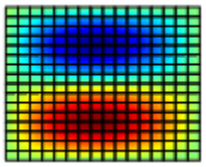	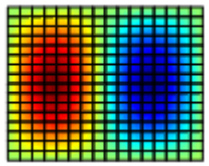	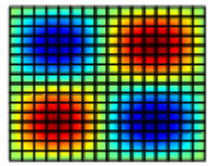
	$\omega_1^* = 2.4796$	$\omega_2^* = 4.1488$	$\omega_3^* = 4.1488$	$\omega_4^* = 4.1950$	$\omega_5^* = 4.2349$	$\omega_6^* = 5.8309$
Type 3	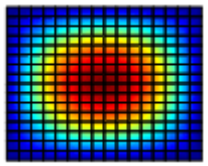	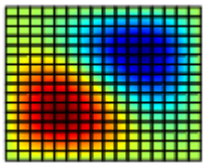	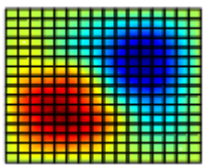	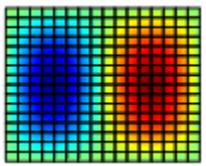	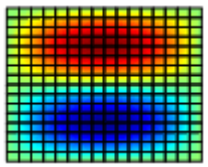	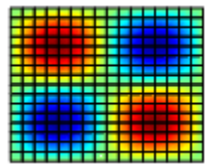
	$\omega_1^* = 3.0882$	$\omega_2^* = 4.1488$	$\omega_3^* = 4.1488$	$\omega_4^* = 4.4663$	$\omega_5^* = 4.5745$	$\omega_6^* = 5.8761$

Figure 8 The first six eigenmodes of FGSW plates (SSSS, $/b = 1, a/h = 10, K_1 = 100, K_2 = 5, \mu = 5$, $k = 1$, scheme 1-3-1, and Pattern.

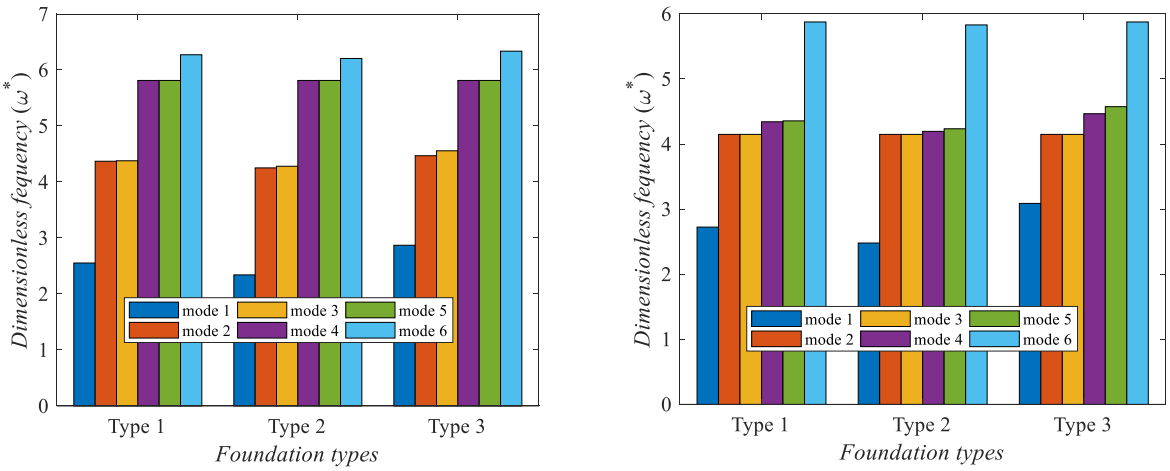

a) Pattern 1 b) Pattern 2

Figure 9 The first six natural frequencies of FGSW plates with different foundation types (SSSS, $/b = 1, a/h = 10, K_1 = 100, K_2 = 5, \mu = 5$, $k = 1$, and scheme 1-3-1).

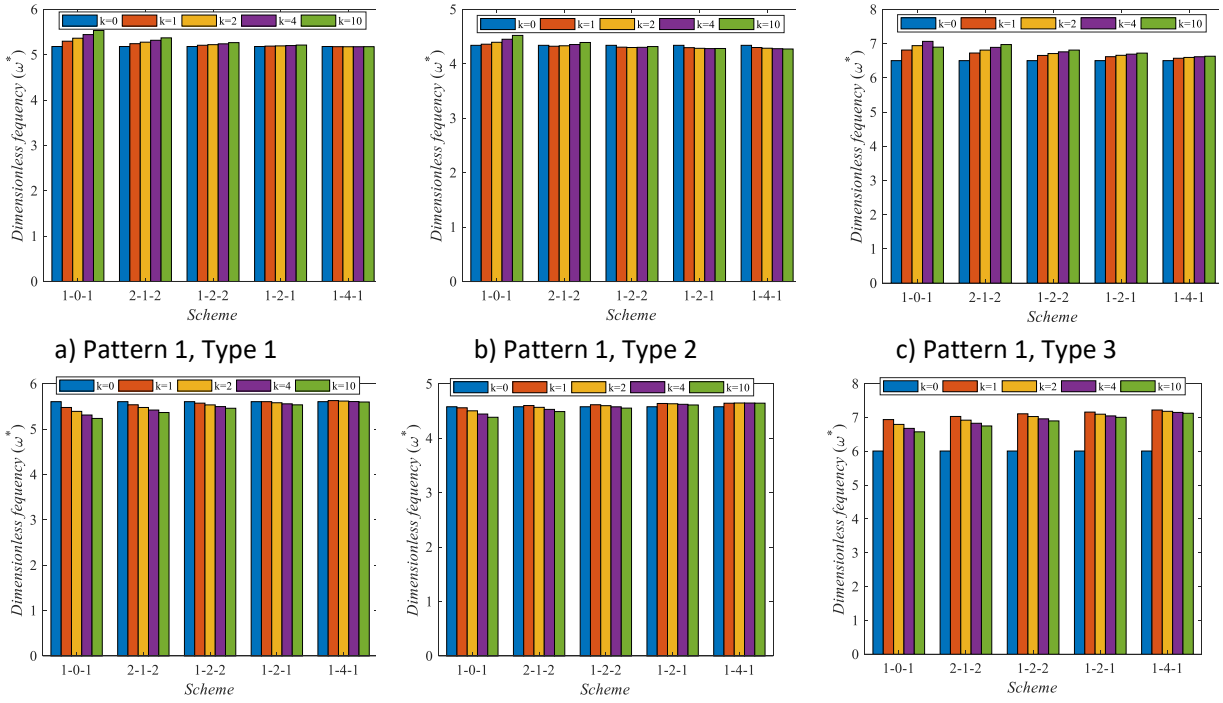

a) Pattern 1, Type 1 b) Pattern 1, Type 2 c) Pattern 1, Type 3

d) Pattern 2, Type 1 e) Pattern 2, Type 2 f) Pattern 2, Type 3

Figure 10 The frequencies of FGSW plates versus schemes and power-law index (CCCC, $a/b = 1, a/h = 20, K_1 = K_2 = 200$, and $\mu = 50$).

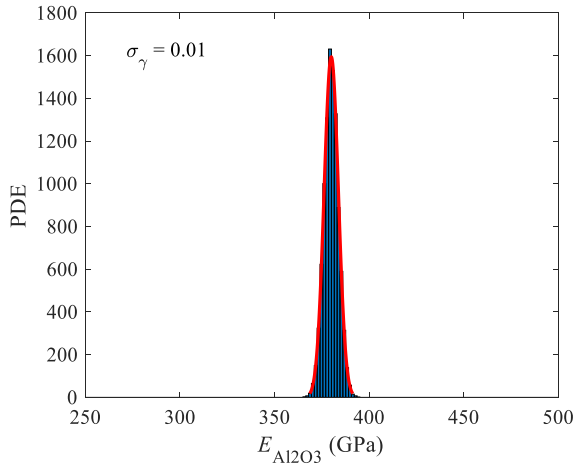

a) $\sigma_\gamma = 0.05$

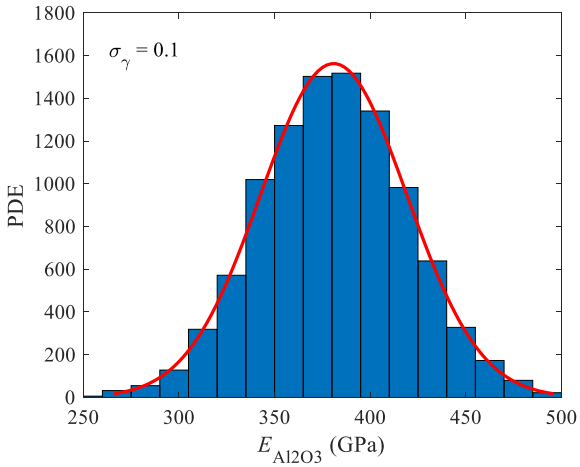

b) $\sigma_\gamma = 0.1$

Figure 11 The PDF of the uncertain variable E_{Al2O3} at different standard deviations.

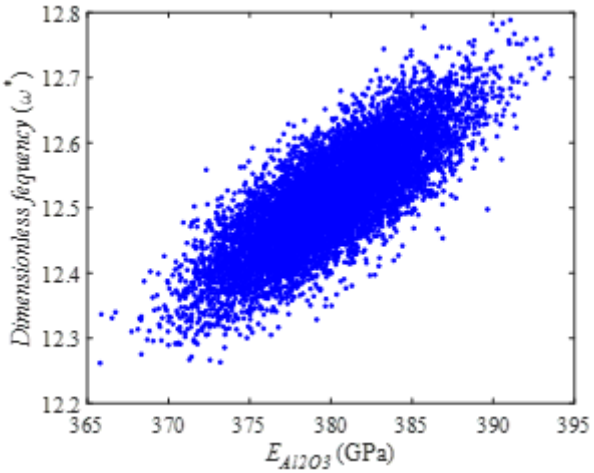

a) The range of natural frequency versus uncertain parameter $E_{\mathrm{Al_2O_3}}$

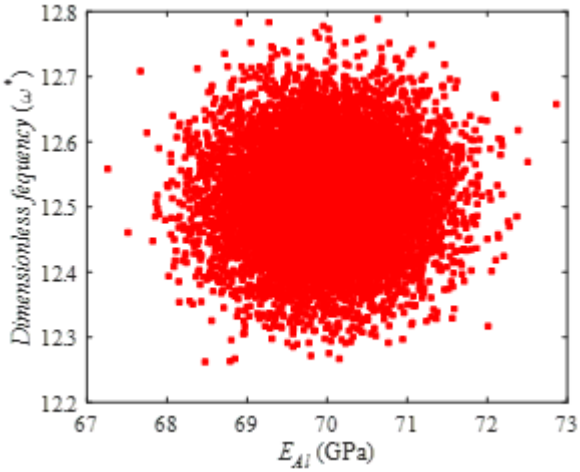

b) The range of natural frequency versus uncertain parameter E_{Al}

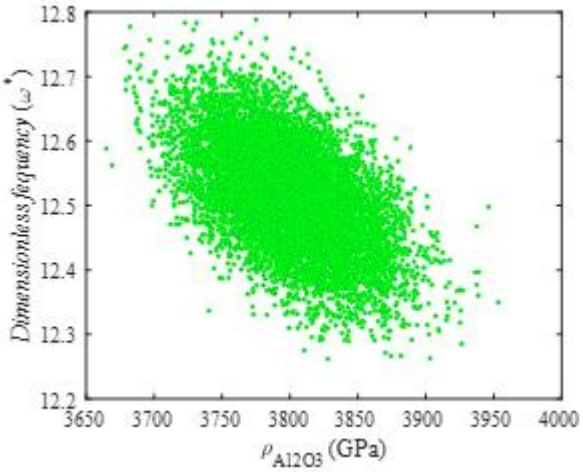

c) The range of natural frequency versus uncertain parameter $\rho_{\mathrm{Al_2O_3}}$

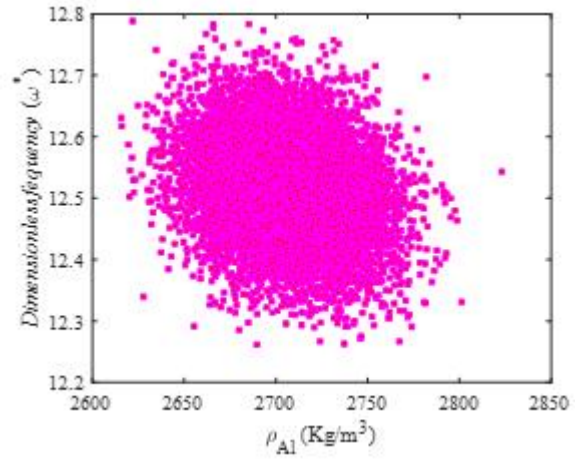

d) The range of natural frequency versus uncertain parameter ρ_{Al}

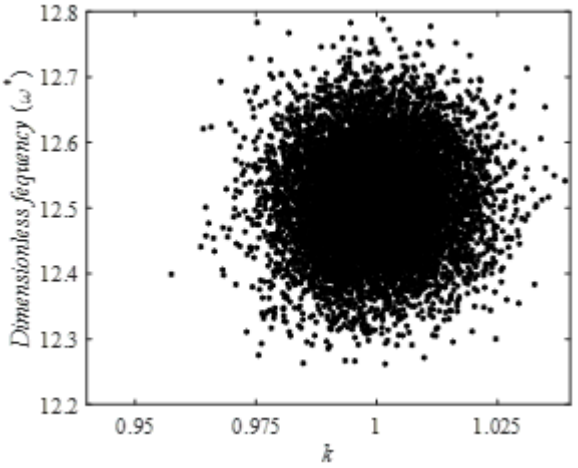

e) The range of natural frequency versus uncertain parameter k

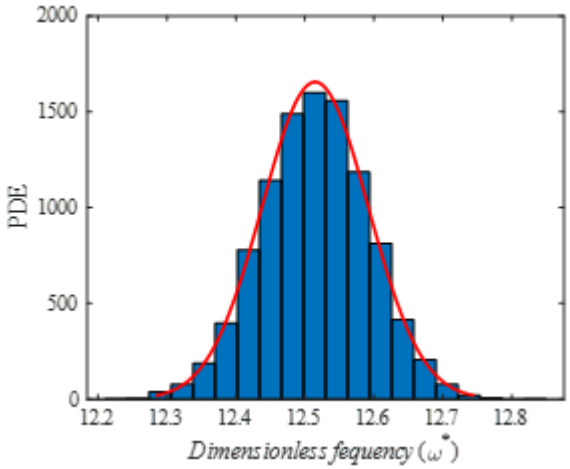

f) The distribution function of the natural frequency ($Sk_\tau = 0.0273; Ku_\tau = 2.9551$)

Figure 12 The natural frequency of FGSW plates with standard deviations $\sigma_\gamma = 0.01$ (SSSS, $a/b = 1, a/h = 25$, $K_1 = 150$, $K_2 = 15, \mu = 20$, scheme 2-1-2, Pattern 1, and Type 1).

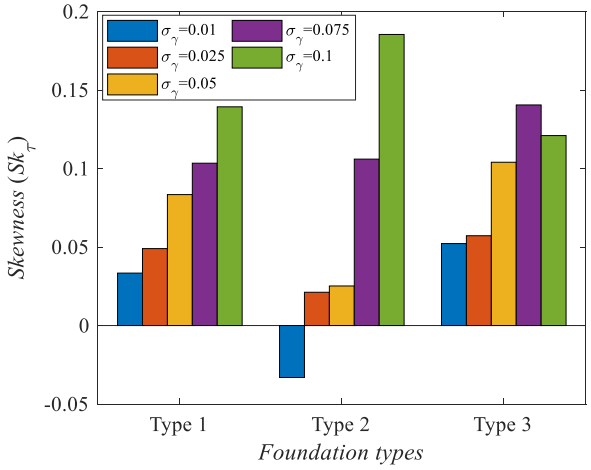

a) Pattern 1 (Skewness)

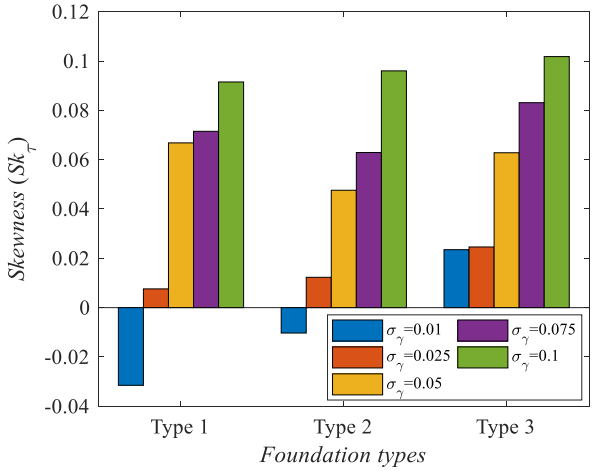

b) Pattern 2 (Skewness)

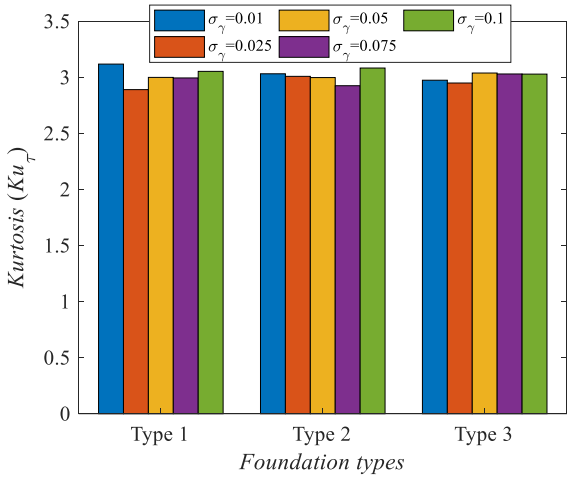

c) Pattern 1 (Kurtosis)

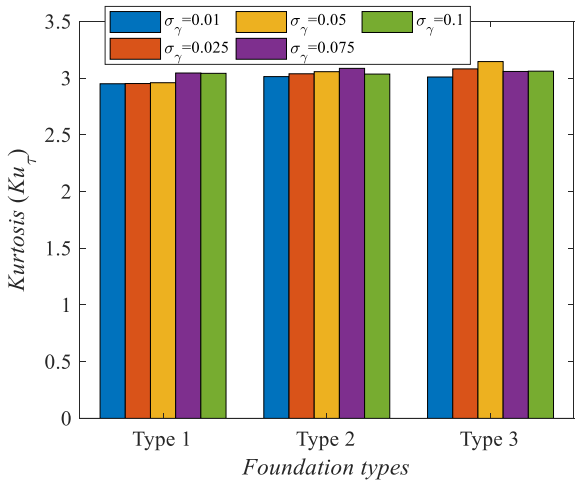

d) Pattern 2 (Kurtosis)

Figure 13 Effect of σ_γ on distribution function of natural frequency of FGSW plates (CCCC, $a/b = 1, a/h = 15$, $K_1 = 200, K_2 = 10, \mu = 15$, and scheme 1-2-1).

Table 4 The dimensionless natural frequencies of FGSW plates (CCCC, $a/b = 1, a/h = 20, K_1 = 200, K_2 = 10$, and $\mu = 10$).

Patterns	Foundation types	Thickness ratio	Power-law index k				
			0	1	2	4	10
Patterns 1	Type 1	1-0-1	5.1801	5.2973	5.3633	5.443	5.5346
		2-1-2	5.1801	5.2427	5.2759	5.3177	5.3708
		1-2-2	5.1801	5.2078	5.2211	5.2393	5.2658
		1-2-1	5.1801	5.1895	5.1939	5.2012	5.2123
		1-4-1	5.1801	5.1765	5.1752	5.1754	5.1765
	Type 2	1-0-1	4.3390	4.3597	4.3950	4.4505	4.5213
		2-1-2	4.3390	4.3223	4.3307	4.3537	4.3913
		1-2-2	4.3390	4.3054	4.2991	4.3024	4.3166
		1-2-1	4.3390	4.2962	4.2842	4.2791	4.2811
		1-4-1	4.3390	4.2990	4.2859	4.2770	4.2717
	Type 3	1-0-1	6.5033	6.8134	6.9416	7.0669	6.8978
		2-1-2	6.5033	6.7261	6.8116	6.8914	6.9734
		1-2-2	6.5033	6.6552	6.7105	6.7603	6.8120
		1-2-1	6.5033	6.6187	6.6589	6.6929	6.7235
		1-4-1	6.5033	6.5731	6.5972	6.6171	6.6324
Pattern 2	Type 1	1-0-1	5.6059	5.4779	5.3918	5.3114	5.2361
		2-1-2	5.6059	5.5372	5.4779	5.4211	5.3665
		1-2-2	5.6059	5.5732	5.5347	5.4974	5.4606
		1-2-1	5.6059	5.6062	5.5819	5.5581	5.5357
		1-4-1	5.6059	5.6297	5.6196	5.6083	5.5985
	Type 2	1-0-1	4.5781	4.5589	4.5032	4.4442	4.3848
		2-1-2	4.5781	4.5999	4.5672	4.5295	4.4892
		1-2-2	4.5781	4.6148	4.5978	4.5766	4.553
		1-2-1	4.5781	4.6381	4.6327	4.6228	4.6106
		1-4-1	4.5781	4.6431	4.6468	4.6461	4.6437
	Type 3	1-0-1	6.0086	6.9380	6.7959	6.6781	6.5762
		2-1-2	6.0086	7.0310	6.9210	6.8295	6.7499
		1-2-2	6.0086	7.1092	7.0281	6.9601	6.8989
		1-2-1	6.0086	7.1600	7.0977	7.0466	7.0046
		1-4-1	6.0086	7.2218	7.1828	7.1500	7.1252

Table 5 The first six dimensionless natural frequencies of FGSW plates ($a/b = 1, a/h = 25, K_1 = 150, K_2 = 5, \mu = 20$, $k = 2$, and Pattern 1).

BCs	Foundation types	Thickness ratio	Dimensionless natural frequencies					
			ω_1^*	ω_2^*	ω_3^*	ω_4^*	ω_5^*	ω_6^*
SSSS	Type 1	1-0-1	4.6294	4.6294	5.6248	6.1306	6.5568	7.0345
		2-1-2	5.0418	5.0418	5.5210	6.0345	6.9649	7.1409
		1-2-2	5.3823	5.3823	5.4475	5.9844	6.9784	7.0792
		1-2-1	5.4109	5.5444	5.5444	5.9608	6.9898	7.0410
		1-4-1	5.3750	5.7700	5.7700	5.9587	7.0121	7.0752
	Type 2	1-0-1	4.1655	4.6294	4.6294	4.8044	5.8889	5.9117
		2-1-2	4.0904	4.7364	5.0418	5.0418	5.8274	5.8485
		1-2-2	4.0404	4.7119	5.3823	5.3823	5.7920	5.8935
		1-2-1	4.0159	4.7017	5.5444	5.5444	5.7751	5.9216
		1-4-1	3.9966	4.7210	5.7700	5.7700	5.7845	6.0373
	Type 3	1-0-1	4.6294	4.6294	6.5568	7.8435	7.8456	8.2470
		2-1-2	5.0418	5.0418	7.1409	7.7064	7.7095	8.1188
		1-2-2	5.3823	5.3823	7.6124	7.6181	7.6230	8.0472
		1-2-1	5.5444	5.5444	7.5647	7.5720	7.8527	8.0115
		1-4-1	5.7700	5.7700	7.5179	7.5292	7.9932	7.9999

SCSC	Type 1	1-0-1	4.6294	5.9511	6.4126	7.2578	7.5053	7.9138
		2-1-2	5.0418	5.858	6.3239	7.1916	7.3894	7.8056
		1-2-2	5.3823	5.8020	6.2845	7.2081	7.3215	7.7590
		1-2-1	5.5444	5.7733	6.2654	7.2203	7.2871	7.7367
		1-4-1	5.7535	5.7700	6.2715	7.2663	7.3053	7.7474
	Type 2	1-0-1	4.4178	4.6294	5.0135	6.0474	6.1598	6.6618
		2-1-2	4.3551	4.9545	5.0418	6.0121	6.0854	6.5963
		1-2-2	4.3261	4.944	5.3823	6.0638	6.0653	6.6011
		1-2-1	4.3118	4.9404	5.5444	6.0557	6.0946	6.6054
		1-4-1	4.3138	4.9724	5.77	6.0801	6.2147	6.6658
	Type 3	1-0-1	4.6294	8.1774	8.3722	8.3735	8.7139	8.7146
		2-1-2	5.0418	8.2436	8.2456	8.5873	8.6042	8.9058
		1-2-2	5.3823	8.1609	8.1656	8.5124	8.5430	9.2080
		1-2-1	5.5444	8.1163	8.1241	8.4719	8.5129	9.1879
		1-4-1	5.7700	8.0722	8.0910	8.4385	8.5101	9.2075
SSCC	Type 1	1-0-1	5.2756	5.967	6.4574	6.4775	7.4064	7.5183
		2-1-2	5.7455	5.8752	6.3946	7.0326	7.3546	7.4035
		1-2-2	5.8216	6.1335	6.366	7.3368	7.3975	7.5076
		1-2-1	5.7942	6.3183	6.3527	7.3034	7.4236	7.7337
		1-4-1	5.7774	6.3725	6.5754	7.2837	7.5405	7.8267
	Type 2	1-0-1	4.4391	5.0960	5.2756	6.1756	6.2250	6.4574
		2-1-2	4.3780	5.0441	5.7455	6.1026	6.2062	6.6664
		1-2-2	4.3522	5.0468	6.0848	6.1335	6.2872	6.6810
		1-2-1	4.3395	5.0502	6.0763	6.3183	6.3338	6.6905
		1-4-1	4.3454	5.0988	6.1027	6.4892	6.5754	6.7616
	Type 3	1-0-1	5.2756	6.4574	7.8572	8.2992	8.3843	8.7677
		2-1-2	5.7455	7.0326	7.7217	8.176	8.257	8.6482
		1-2-2	6.1335	7.5074	7.6311	8.1138	8.1774	8.5879
		1-2-1	6.3183	7.5852	7.7337	8.0835	8.1351	8.5567
		1-4-1	6.5754	7.543	8.0484	8.0789	8.0983	8.5477
CCCC	Type 1	1-0-1	5.9855	6.5523	7.5324	7.5756	8.0294	8.6816
		2-1-2	5.8955	6.4769	7.4196	7.5410	7.9328	8.5676
		1-2-2	5.8452	6.4620	7.3567	7.6142	7.9070	8.5301
		1-2-1	5.8195	6.4562	7.3250	7.6571	7.8962	8.5170
		1-4-1	5.8070	6.4935	7.3104	7.8116	7.9332	8.5626
	Type 2	1-0-1	4.4639	5.1906	6.1941	6.4241	6.7998	7.6645
		2-1-2	4.4051	5.1478	6.1228	6.4252	6.7475	7.5954
		1-2-2	4.3836	5.1671	6.1084	6.5407	6.7758	7.6126
		1-2-1	4.3731	5.1795	6.1019	6.6057	6.7929	7.6261
		1-4-1	4.3846	5.2489	6.1334	6.8021	6.8826	7.7201
	Type 3	1-0-1	8.3968	8.3984	8.8173	8.8297	8.8641	8.8641
		2-1-2	8.2704	8.2728	8.7005	8.7189	9.5180	9.5705
		1-2-2	8.1917	8.1971	8.6437	8.6769	9.4650	9.5293
		1-2-1	8.1492	8.1579	8.6131	8.6573	9.4186	9.5339
		1-4-1	8.1100	8.1304	8.6030	8.6791	9.4023	9.6119

Table 6 The first six dimensionless natural frequencies of FGSW plates ($a/b = 1, a/h = 25, K_1 = 150, K_2 = 5, \mu = 20, k = 2$, and Pattern 2).

BCs	Foundation types	Thickness ratio	Dimensionless natural frequencies					
			ω_1^*	ω_2^*	ω_3^*	ω_4^*	ω_5^*	ω_6^*
SSSS	Type 1	1-0-1	5.5421	5.5421	5.5809	6.2713	7.3073	7.6308
		2-1-2	5.2185	5.2185	5.686	6.3741	7.391	7.4383
		1-2-2	4.8497	4.8497	5.7672	6.4291	6.8686	7.5308
		1-2-1	4.6259	4.6259	5.8298	6.4914	6.5518	7.6079
		1-4-1	4.2368	4.2368	5.8914	6.0007	6.5223	7.6719
	Type 2	1-0-1	4.1713	5.0222	5.5421	5.5421	6.1009	6.6105
		2-1-2	4.2471	5.0966	5.2185	5.2185	6.1981	6.6674
		1-2-2	4.2999	4.8497	4.8497	5.1201	6.2456	6.6136
		1-2-1	4.3457	4.6259	4.6259	5.1665	6.3034	6.5518
		1-4-1	4.2368	4.2368	4.3837	5.1697	6.0007	6.3242
	Type 3	1-0-1	5.5421	5.5421	7.7986	7.8164	7.8494	8.3485
		2-1-2	5.2185	5.2185	7.391	7.9437	7.9614	8.494
		1-2-2	4.8497	4.8497	6.8686	8.0559	8.0721	8.5898
		1-2-1	4.6259	4.6259	6.5518	8.1408	8.1566	8.6743
		1-4-1	4.2368	4.2368	6.0007	8.2241	8.2367	8.5145
SCSC	Type 1	1-0-1	5.5421	5.9896	6.5926	7.5762	7.8502	8.1538
		2-1-2	5.2185	6.0887	6.69	7.6985	7.931	8.2696
		1-2-2	4.8497	6.156	6.7367	7.7781	7.9112	8.3215
		1-2-1	4.6259	6.2097	6.7903	7.8454	7.9564	8.1712
		1-4-1	4.2368	6.252	6.8091	7.4839	7.8954	7.9024
	Type 2	1-0-1	4.5307	5.2924	5.5421	6.4222	6.7872	7.1172
		2-1-2	4.5996	5.2185	5.3607	6.5089	6.8392	7.1975
		1-2-2	4.6351	4.8497	5.3733	6.5392	6.7800	7.1976
		1-2-1	4.6259	4.6730	5.4120	6.5856	6.8103	7.2414
		1-4-1	4.2368	4.6889	5.4010	6.5872	6.7194	7.2100
	Type 3	1-0-1	5.5421	8.3411	8.4029	8.7518	8.9129	9.6879
		2-1-2	5.2185	8.4877	8.5357	8.9000	9.0368	9.2178
		1-2-2	4.8497	8.5642	8.6009	8.6289	9.0058	9.0993
		1-2-1	4.6259	8.1712	8.6760	8.6959	8.7081	9.0827
		1-4-1	4.2368	7.4839	7.9756	8.5145	8.7476	8.7540
SSCC	Type 1	1-0-1	6.0209	6.3156	6.7248	7.5911	7.7304	8.1449
		2-1-2	5.9468	6.119	6.8162	7.2790	7.7145	8.2082
		1-2-2	5.5266	6.1834	6.7645	6.8498	7.7955	8.1576
		1-2-1	5.2716	6.2365	6.4525	6.8992	7.8627	8.1892
		1-4-1	4.8282	5.9098	6.2757	6.9043	7.9122	8.1046
	Type 2	1-0-1	4.5718	5.4560	6.3156	6.4450	7.1263	7.2303
		2-1-2	4.6394	5.5172	5.9468	6.5320	7.1590	7.2790
		1-2-2	4.6714	5.5142	5.5266	6.5623	6.7645	7.0661
		1-2-1	4.7085	5.2716	5.5479	6.4525	6.6083	7.0811
		1-4-1	4.7205	4.8282	5.5206	5.9098	6.6084	6.9563
	Type 3	1-0-1	6.3156	7.7304	7.8329	8.3912	8.4714	8.9272
		2-1-2	5.9468	7.279	7.9768	8.5312	8.6085	9.0596
		1-2-2	5.5266	6.7644	8.0857	8.6331	8.6872	9.1348
		1-2-1	5.2716	6.4525	8.1696	8.7046	8.7667	9.2031
		1-4-1	4.8282	5.9098	8.2486	8.7016	8.7677	8.8108
CCCC	Type 1	1-0-1	6.0608	6.8837	7.6343	8.3944	8.4820	9.0970
		2-1-2	6.1572	6.9665	7.7538	8.4960	8.5209	9.1913
		1-2-2	6.2176	6.9829	7.8274	8.4327	8.5217	9.1991
		1-2-1	6.2696	7.0264	7.8928	8.4466	8.5766	8.8574
		1-4-1	6.3045	7.0142	7.9365	8.1124	8.1124	8.3266

	Type 2	1-0-1	4.6242	5.6506	6.4913	7.3925	7.5089	8.2984
		2-1-2	4.6897	5.7019	6.5747	7.4569	7.5154	8.3625
		1-2-2	4.7166	5.6789	6.5981	7.3821	7.4283	8.3246
		1-2-1	4.7522	5.7055	6.6422	7.3773	7.4605	8.3588
		1-4-1	4.7587	5.6578	6.6367	7.214	7.4005	8.1124
	Type 3	1-0-1	8.3914	8.4556	8.9710	9.1339	9.8658	10.2068
		2-1-2	8.5363	8.5859	9.1085	9.2451	9.9877	9.9920
		1-2-2	8.6453	8.6714	9.1878	9.2836	9.2858	9.2884
		1-2-1	8.7187	8.7392	8.8574	8.8574	9.2603	9.3401
		1-4-1	8.1124	8.1124	8.7851	8.7917	9.2985	9.3458

Table 7 The characteristics of input parameters.

No.	Parameters	Unit	Law of distribution	Deterministic value	Uncertain parameter $(\overline{\gamma_i}, \sigma_{\gamma_i})$
1	E_{Al}	GPa	Standard distribution	-	(70, 0.01 or 0.1)
2	$E_{\mathrm{Al_2O_3}}$	GPa	Standard distribution	-	(380, 0.01 or 0.1)
3	ρ_{Al}	kg/m^3	Standard distribution	-	(2707, 0.01 or 0.1)
4	$\rho_{\mathrm{Al_2O_3}}$	kg/m^3	Standard distribution	-	(3800, 0.01 or 0.1)
5	k	-	Standard distribution	-	(1, 0.01 or 0.1)
6	υ_{Al}	-	-	0.3	-
7	$\upsilon_{\mathrm{Al_2O_3}}$	-	-	0.3	-

Table 8 Effect of σ_γ on distribution function of natural frequency of FGSW plates (CCCC, $a/b = 1, a/h = 15, K_1 = 200, K_2 = 10, \mu = 15$, and scheme 1-2-1).

Patterns	Foundation types	The standard deviation				
		$\sigma_\gamma = 0.01$	$\sigma_\gamma = 0.025$	$\sigma_\gamma = 0.05$	$\sigma_\gamma = 0.075$	$\sigma_\gamma = 0.1$
Pattern 1	Type 1	0.0334[(a)]	0.049	0.0834	0.1034	0.1393
		2.9512[(b)]	2.9534	2.9605	3.0461	3.0433
	Type 2	-0.0331[(a)]	0.0212	0.0252	0.106	0.1854
		3.0144[(b)]	3.0392	3.0578	3.0871	3.0368
	Type 3	0.0522[(a)]	0.0572	0.104	0.1405	0.121
		3.011[(b)]	3.0823	3.1469	3.0598	3.0624
Pattern 2	Type 1	-0.0315[(a)]	0.0076	0.0668	0.0715	0.0915
		3.1181[(b)]	2.8904	2.9994	2.9945	3.0532
	Type 2	-0.0103[(a)]	0.0123	0.0476	0.0629	0.096
		3.0316[(b)]	3.0088	2.9979	2.9252	3.083
	Type 3	0.0235[(a)]	0.0246	0.0628	0.0831	0.1018
		2.9742[(b)]	2.9494	3.0383	3.0299	3.0288

Note that: [(a)] The skewness of the distribution; [(b)] The kurtosis of the distribution.

4 CONCLUSIONS

This study presents an enhanced approach that integrates a simple finite element technique based on the Q4 element with the improved first-order shear deformation theory to investigate the natural frequencies of FGSW plates resting on a variable elastic foundation. Additionally, Monte Carlo Simulation is employed to analyze the impact of uncertain input parameters on the natural frequencies. The results yield several noteworthy points, including:

- The proposed factor facilitates the transformation of mathematical formulas, thereby reducing the overall analysis time. This advantage becomes particularly significant when used in conjunction with Monte Carlo Simulation, which typically demands substantial computational time and storage resources.
- FGSW plates with a hardcore exhibit greater bending stiffness compared to those with a softcore. However, in vibration-related problems, the natural frequency is influenced by both the stiffness and the overall mass

of the sandwich plates. Consequently, in many cases, FGSW plates with a softcore may outperform those with a hardcore due to their lower mass, which can lead to higher natural frequencies.

- VEF significantly affects the natural frequency of FGSW plate, the deformation field of the plate depends on the support of different types of foundation.
- In general, the power-law index reduces the stiffness and alters the mass distribution of the structure. By adjusting the value of the power-law index k, it is possible to tailor the material gradation and mechanical behavior to achieve desired structural properties.
- The standard deviation of the input uncertain variable has a significant influence on the uncertainty associated with the natural frequency of FGSW plates. An increase in the standard deviation leads to a corresponding rise in the variability of the natural frequency.
- Although Monte Carlo Simulation is conceptually straightforward, it is computationally intensive and time-consuming. Therefore, future research could aim to improve the efficiency of MCS by incorporating advanced sampling strategies, intelligent computational methods leveraging artificial intelligence (AI), and other innovative approaches.
- The numerical results presented in this study can assist engineers in the analysis and design of FGSW plates, particularly in situations where input parameters may be uncertain or imprecise.

Author's Contributions: Writing - Reviewing & Editing, Supervision, Project administration, Methodology, Nhan Thinh Hoang; Investigation, Writing Original draft, Software, Formal analysis , Ngoc-Tu Do.

Editor: Rogério José Marczak

References

Akavci, SS. (2016). Mechanical behavior of functionally graded sandwich plates on elastic foundation. *Composites Part B: Engineering, 96*, 136-152.

Akbaba, Öner Murat, Yıldırım, Bora, & Canbaloğlu, Güvenç. (2022). Vibration based fatigue analysis of a structure integrated on an air vehicle by using experimental and theoretical methods. *Results in Engineering, 15*, 100549.

Alibeigloo, A, & Alizadeh, M. (2015). Static and free vibration analyses of functionally graded sandwich plates using state space differential quadrature method. *European Journal of Mechanics-A/Solids, 54*, 252-266.

Avcar, Mehmet, & Mohammed, Waleed Khalid Mohammed. (2018). Free vibration of functionally graded beams resting on Winkler-Pasternak foundation. *Arabian Journal of Geosciences, 11*(10), 232.

Baferani, A Hasani, Saidi, AR, & Ehteshami, H. (2011). Accurate solution for free vibration analysis of functionally graded thick rectangular plates resting on elastic foundation. *Composite Structures, 93*(7), 1842-1853.

Belabed, Zakaria, Bousahla, Abdelmoumen Anis, Houari, Mohammed Sid Ahmed, Tounsi, Abdelouahed, & Mahmoud, SR. (2018). A new 3-unknown hyperbolic shear deformation theory for vibration of functionally graded sandwich plate. *Earthquakes and Structures, 14*(2), 103-115.

Belabed, Zakaria, Tounsi, Abdelouahed, Al-Osta, Mohammed A, Tounsi, Abdeldjebbar, & Minh, Hoang-Le. (2024). On the elastic stability and free vibration responses of functionally graded porous beams resting on Winkler-Pasternak foundations via finite element computation. *Geomechanics and Engineering, 36*(2), 183.

Bouadi, Abed, Bousahla, Abdelmoumen Anis, Houari, Mohammed Sid Ahmed, Heireche, Houari, & Tounsi, Abdelouahed. (2018). A new nonlocal HSDT for analysis of stability of single layer graphene sheet. *Advances in nano research, 6*(2), 147.

Bounouara, Fatima, Aldosari, Salem Mohammed, Chikh, Abdelbaki, Kaci, Abdelhakim, Bousahla, Abdelmoumen Anis, Bourada, Fouad, . . . Albalawi, Hind. (2023). The effect of visco-Pasternak

foundation on the free vibration behavior of exponentially graded sandwich plates with various boundary conditions. *Steel and Composite Structures, An International Journal, 46*(3), 367-383.

Clough, Ray W. (1960). The finite element in plane stress analysis. *Proc. 2^< nd> ASCE Confer. On Electric Computation, 1960*.

Djilali, Nassira, Bousahla, Abdelmoumen Anis, Kaci, Abdelhakim, Selim, Mahmoud M, Bourada, Fouad, Tounsi, Abdeldjebbar, . . . Mahmoud, SR. (2022). Large cylindrical deflection analysis of FG carbon nanotube-reinforced plates in thermal environment using a simple integral HSDT. *Steel and Composite Structures, An International Journal, 42*(6), 779-789.

Do, Ngoc-Tu, Nguyen, Truong Thanh, Tran, Trung Thanh, Le, Pham Binh, & Pham, Quoc-Hoa. (2023). Free vibration analysis of bio-inspired helicoid laminated composite plates resting on elastic foundation using isogeometric analysis and artificial neural network. *Mechanics of Time-Dependent Materials*, 1-24.

Do, Ngoc-Tu, & Pham, Quoc-Hoa. (2023). Vibration and dynamic control of piezoelectric functionally graded porous plates in the thermal environment using FEM and Shi's TSDT. *Case Studies in Thermal Engineering, 47*, 103105.

Do, Ngoc-Tu, & Tran, Trung Thanh. (2024). Random vibration analysis of FGM plates subjected to moving load using a refined stochastic finite element method. *Defence Technology, 34*, 42-56.

Ferreira, António JM. (2009). *MATLAB codes for finite element analysis*: Springer.

Gawah, Qais, Bourada, Fouad, Al-Osta, Mohammed A, Tahir, Saeed I, Tounsi, Abdelouahed, & Yaylacı, Murat. (2024). An improved first-order shear deformation theory for wave propagation analysis in FG-CNTRC beams resting on a viscoelastic substrate.

Hosseini-Hashemi, Sh, Taher, H Rokni Damavandi, Akhavan, H, & Omidi, M. (2010). Free vibration of functionally graded rectangular plates using first-order shear deformation plate theory. *Applied Mathematical Modelling, 34*(5), 1276-1291.

Kapur, KC, & Lamberson, LR. (1977). Reliability in Engineering Design John Wiley & Sons. *New York*, 213-213.

Katsikadelis, JOHN T, & Armenakas, AE. (1984). Plates on elastic foundation by BIE method. *Journal of Engineering Mechanics, 110*(7), 1086-1105.

Keshtegar, Behrooz, Motezaker, Mohsen, Kolahchi, Reza, & Trung, Nguyen-Thoi. (2020). Wave propagation and vibration responses in porous smart nanocomposite sandwich beam resting on Kerr foundation considering structural damping. *Thin-Walled Structures, 154*, 106820.

Lafi, Djamel Eddine, Bouhadra, Abdelhakim, Mamen, Belgacem, Menasria, Abderahmane, Bourada, Mohamed, Bousahla, Abdelmoumen Anis, . . . Yaylaci, Murat. (2024). Combined influence of variable distribution models and boundary conditions on the thermodynamic behavior of FG sandwich plates lying on various elastic foundations. *Structural Engineering and Mechanics, 89*(2), 103.

Le, Truong Son, Tran, Trung Thanh, Pham, Chung, & Pham, Quoc Hoa. (2025). Free vibration analysis of functionally graded sandwich spherical shells with honeycomb core resting on Kerr foundation using the MITC4 element. *Nondestructive Testing and Evaluation, 40*(3), 1161-1179.

Li, Q, Iu, VP, & Kou, KP. (2008). Three-dimensional vibration analysis of functionally graded material sandwich plates. *Journal of Sound and Vibration, 311*(1-2), 498-515.

Liu, Ning, & Jeffers, Ann E. (2017). Isogeometric analysis of laminated composite and functionally graded sandwich plates based on a layerwise displacement theory. *Composite Structures, 176*, 143-153.

Luat, Doan Trac, Van Thom, Do, Thanh, Tran Trung, Van Minh, Phung, Van Ke, Tran, & Van Vinh, Pham. (2021). Mechanical analysis of bi-functionally graded sandwich nanobeams. *Advances in nano research, 11*(1), 55-71.

Mantari, JL, & Soares, C Guedes. (2013). A novel higher-order shear deformation theory with stretching effect for functionally graded plates. *Composites Part B: Engineering, 45*(1), 268-281.

Mudhaffar, Ismail M, Chikh, Abdelbaki, Tounsi, Abdelouahed, Al-Osta, Mohammed A, Al-Zahrani, Mesfer M, & Al-Dulaijan, Salah U. (2023). Impact of viscoelastic foundation on bending behavior of FG plate subjected to hygro-thermo-mechanical loads. *Structural Engineering and Mechanics, An Int'l Journal, 86*(2), 167-180.

Natarajan, S, & Manickam, Ganapathi. (2012). Bending and vibration of functionally graded material sandwich plates using an accurate theory. *Finite Elements in Analysis and Design, 57*, 32-42.

Neves, AMA, Ferreira, AJM, Carrera, Erasmo, Cinefra, Maria, Roque, CMC, Jorge, RMN, & Soares, CM Mota. (2013). Static, free vibration and buckling analysis of isotropic and sandwich functionally graded plates using a quasi-3D higher-order shear deformation theory and a meshless technique. *Composites Part B: Engineering, 44*(1), 657-674.

Neves, AMA, Ferreira, AJM, Carrera, Erasmo, Cinefra, Maria, Roque, CMC, Jorge, RMN, & Soares, CMM. (2012). A quasi-3D hyperbolic shear deformation theory for the static and free vibration analysis of functionally graded plates. *Composite Structures, 94*(5), 1814-1825.

Neves, AMA, Ferreira, Antonio JM, Carrera, Erasmo, Cinefra, Maria, Jorge, Renato Manuel Natal, Mota Soares, CM, & Araújo, Aurélio L. (2017). Influence of zig-zag and warping effects on buckling of functionally graded sandwich plates according to sinusoidal shear deformation theories. *Mechanics of Advanced Materials and Structures, 24*(5), 360-376.

Neves, AMA, Ferreira, Antonio JM, Carrera, Erasmo, Cinefra, Maria, Jorge, RMN, & Soares, CMM. (2012). Static analysis of functionally graded sandwich plates according to a hyperbolic theory considering Zig-Zag and warping effects. *Advances in Engineering Software, 52*, 30-43.

Nguyen, Hoang Nam, Hong, Tran Thi, Vinh, Pham Van, Quang, Nguyen Dinh, & Thom, Do Van. (2019). A refined simple first-order shear deformation theory for static bending and free vibration analysis of advanced composite plates. *Materials, 12*(15), 2385.

Nguyen, Truong Thanh, Le, Truong Son, Tran, Trung Thanh, & Pham, Quoc-Hoa. (2024). Buckling analysis of functionally graded porous variable thickness plates resting on Pasternak foundation using ES-MITC3. *Latin American Journal of Solids and Structures, 21*, e524.

Nguyen, Van Chinh, Tran, Trung Thanh, Nguyen-Thoi, Trung, & Pham, Quoc-Hoa. (2022). A novel finite element formulation for static bending analysis of functionally graded porous sandwich plates. *Frontiers of Structural and Civil Engineering, 16*(12), 1599-1620.

Nguyen, Van Chinh, Tran, Trung Thanh, Sobhy, Mohammed, Hoang, Nhan Thinh, & Hoa Pham, Quoc. (2025). The effective finite element method for free and forced vibration analysis of 2D-FGSW plates lying an elastic foundation. *Mechanics Based Design of Structures and Machines, 53*(2), 1329-1350.

Pham, Quoc-Hoa, Nguyen, Phu-Cuong, & Tran, Trung Thanh. (2022). Free vibration response of auxetic honeycomb sandwich plates using an improved higher-order ES-MITC3 element and artificial neural network. *Thin-Walled Structures, 175*, 109203.

Pham, Quoc-Hoa, Tran, Trung Thanh, & Nguyen, Phu-Cuong. (2023a). Dynamic response of functionally graded porous-core sandwich plates subjected to blast load using ES-MITC3 element. *Composite Structures, 309*, 116722.

Pham, Quoc-Hoa, Tran, Trung Thanh, & Nguyen, Phu-Cuong. (2023b). Uncertain vibration characteristics of Bi-directional functionally graded sandwich nanoplate subjected to dynamic load. *Thin-Walled Structures, 193*, 111206.

Pham, Quoc Hoa, Tran, Trung Thanh, Zenkour, Ashraf M, & Nguyen-Thoi, Trung. (2023). Multi-objective optimization for free vibration of L-shaped bi-functionally graded sandwich plates using an effective finite element method and non-dominated sorting genetic algorithm II. *Composite Structures, 326*, 117622.

Pradhan, SC, & Murmu, T. (2009). Thermo-mechanical vibration of FGM sandwich beam under variable elastic foundations using differential quadrature method. *Journal of Sound and Vibration, 321*(1-2), 342-362.

Reddy, JN. (2000). Analysis of functionally graded plates. *International Journal for numerical methods in engineering, 47*(1-3), 663-684.

Reddy, JN. (2011). A general nonlinear third-order theory of functionally graded plates. *International Journal of Aerospace and Lightweight Structures (IJALS), 1*(1).

Reddy, Junuthula Narasimha. (2003). *Mechanics of laminated composite plates and shells: theory and analysis*: CRC press.

Shahsavari, Davood, Shahsavari, Maryam, Li, Li, & Karami, Behrouz. (2018). A novel quasi-3D hyperbolic theory for free vibration of FG plates with porosities resting on Winkler/Pasternak/Kerr foundation. *Aerospace Science and Technology, 72*, 134-149.

Smith, Ralph C. (2024). *Uncertainty quantification: theory, implementation, and applications*: SIAM.

Sobhy, Mohammed, & Al Mukahal, Fatemah HH. (2023). Magnetic control of vibrational behavior of smart FG sandwich plates with honeycomb core via a quasi-3D plate theory. *Advanced Engineering Materials, 25*(13), 2300096.

Talha, Mohammad, & Singh, BN26596511201. (2010). Static response and free vibration analysis of FGM plates using higher order shear deformation theory. *Applied Mathematical Modelling, 34*(12), 3991-4011.

Thai, Chien H, Nguyen-Xuan, Hung, & Phung-Van, Phuc. (2023). A size-dependent isogeometric analysis of laminated composite plates based on the nonlocal strain gradient theory. *Engineering with Computers*, 1-15.

Thai, Huu-Tai, & Kim, Seung-Eock. (2013). A simple higher-order shear deformation theory for bending and free vibration analysis of functionally graded plates. *Composite Structures, 96*, 165-173.

Thai, Huu-Tai, Nguyen, Trung-Kien, Vo, Thuc P, & Lee, Jaehong. (2014). Analysis of functionally graded sandwich plates using a new first-order shear deformation theory. *European Journal of Mechanics-A/Solids, 45*, 211-225.

Thanh, Tran Trung, Van Ke, Tran, Hoa, Pham Quoc, & Trung, Nguyen Thoi. (2021). An edge-based smoothed finite element for buckling analysis of functionally graded material variable-thickness plates. *Vietnam Journal of Mechanics, 43*(3), 221-235.

Tounsi, Abdeldjebbar, Bousahla, Abdelmoumen Anis, Tahir, Saeed I, Mostefa, Adda Hadj, Bourada, Fouad, Al-Osta, Mohammed A, & Tounsi, Abdelouahed. (2024). Influences of Different Boundary Conditions and Hygro-Thermal Environment on the Free Vibration Responses of FGM Sandwich Plates Resting on Viscoelastic Foundation. *International Journal of Structural Stability & Dynamics, 24*(11).

Tounsi, Abdeldjebbar, Mostefa, Adda Hadj, Attia, Amina, Bousahla, Abdelmoumen Anis, Bourada, Fouad, Tounsi, Abdelouahed, & Al-Osta, Mohammed A. (2023). Free vibration investigation of functionally graded plates with temperaturedependent properties resting on a viscoelastic foundation. *Structural Engineering and Mechanics, An Int'l Journal, 86*(1), 1-16.

Tounsi, Abdeldjebbar, Mostefa, Adda Hadj, Bousahla, Abdelmoumen Anis, Tounsi, Abdelouahed, Ghazwani, Mofareh Hassan, Bourada, Fouad, & Bouhadra, Abdelhakim. (2023). Thermodynamical bending analysis of P-FG sandwich plates resting on nonlinear visco-Pasternak's elastic foundations. *Steel and Composite Structures, 49*(3), 307-323.

Tran, Trung Thanh, & Le, Pham Binh. (2023). Nonlocal dynamic response analysis of functionally graded porous L-shape nanoplates resting on elastic foundation using finite element formulation. *Engineering with Computers, 39*(1), 809-825.

Tran, Trung Thanh, & Truong Thi Huong, Huyen. (2024). The nonlinear free vibration analysis-based an enhanced finite element procedure of tri-functionally graded sandwich plates with a square central cutout. *Mechanics Based Design of Structures and Machines*, 1-23.

Tran, Trung Thanh, Zenkour, Ashraf M, & Pham, Quoc Hoa. (2025). The nonlinear vibration analysis-based an enhanced finite element procedure of multi-functionally graded sandwich plates. *Thin-Walled Structures*, 113042.

Uddin, MJ, Rasel, SK, Adewole, Jimoh K, & Al Kalbani, Khamis S. (2022). Finite element simulation on the convective double diffusive water-based copper oxide nanofluid flow in a square cavity having vertical wavy surfaces in presence of hydro-magnetic field. *Results in Engineering, 13*, 100364.

Vu, Ngoc Anh, Pham, Thanh Dong, Tran, Trung Thanh, & Pham, Quoc-Hoa. (2023). Third-order isogeometric analysis for vibration characteristics of FGP plates in the thermal environment supported by Kerr foundation. *Case Studies in Thermal Engineering, 45*, 102890.

Yaghoobi, Hessameddin, & Fereidoon, Abdolhossein. (2014). Mechanical and thermal buckling analysis of functionally graded plates resting on elastic foundations: An assessment of a simple refined nth-order shear deformation theory. *Composites Part B: Engineering, 62*, 54-64.

Zarga, Djaloul. (2019). Thermomechanical bending study for functionally graded sandwich plates using a simple quasi-3D shear deformation theory. *Steel and Composite Structures, An International Journal, 32*(3), 389-410.

Zenkour, AM. (2005). A comprehensive analysis of functionally graded sandwich plates: Part 1—Deflection and stresses. *International journal of solids and structures, 42*(18-19), 5224-5242.

Zenkour, Ashraf M. (2006). Generalized shear deformation theory for bending analysis of functionally graded plates. *Applied Mathematical Modelling, 30*(1), 67-84.

Zenkour, Ashraf M. (2013a). Bending analysis of functionally graded sandwich plates using a simple four-unknown shear and normal deformations theory. *Journal of Sandwich Structures & Materials, 15*(6), 629-656.

Zenkour, Ashraf M. (2013b). A simple four-unknown refined theory for bending analysis of functionally graded plates. *Applied Mathematical Modelling, 37*(20-21), 9041-9051.